Muscleblind regulates *Drosophila Dscam2* cell-type-specific alternative splicing

Joshua Shing Shun Li and S. Sean Millard.

School of Biomedical Sciences, The University of Queensland, Brisbane, 4072, Australia.

Correspondence: s.millard@uq.edu.au

Summary

Alternative splicing of genes increases the number of distinct proteins in a cell. In the brain it is highly prevalent, presumably because proteome diversity is crucial for establishing the complex circuitry between trillions of neurons. To provide individual cells with different repertoires of protein isoforms, however, this process must be regulated. Previously, we found that the mutually exclusive alternative splicing of *Drosophila Dscam2* exon 10A and 10B is tightly regulated and crucial for maintaining axon terminal size, dendritic morphology and synaptic numbers. Here, we show that *Drosophila muscleblind* (*mbl*), a conserved splicing factor implicated in myotonic dystrophy, controls *Dscam2* alternative splicing. Removing *mbl* from cells that normally express isoform B induces the expression of isoform A and eliminates the expression of B, demonstrating that Mbl represses one alternative exon and selects the other. Consistent with these observations, we show that *mbl* expression is cell-type-specific and correlates with the expression of isoform B. Our study demonstrates how cell-type-specific expression of a splicing factor can provide neurons with unique protein isoforms.

Introduction

Alternative splicing occurs in approximately 95% of human genes and generates proteome diversity much needed for brain wiring (Pan et al., 2008; Wang et al., 2008). Specifying neuronal connections through alternative splicing would require regulated expression of isoforms with unique functions in different cell types to carry out distinct processes. Although there are some examples of neuronal cell-type-specific isoform expression (Bell et al., 2004; Iijima et al., 2014; Lah et al., 2014; Norris et al., 2014; Schreiner et al., 2014; Tomioka et al., 2016), the mechanisms underlying these deterministic splicing events remain understudied. This is due, in part, to the technical difficulties of assessing isoform expression at the single cell level. Another obstacle is that most splicing regulators are proposed to be ubiquitously expressed (Nilsen and Graveley, 2010), therefore it is not immediately clear how cell-type specific expression would be achieved. For example, the broadly expressed SR and heterogeneous nuclear ribonucleoproteins (hnRNPs) typically have opposing activities, and the prevalence of splice site usage is thought to be controlled by their relative abundances within the cell (Blanchette et al., 2009). There are many notable examples where splicing regulators are expressed in a tissue-specific manner (Calarco et al., 2009; Kuroyanagi et al., 2006; Markovtsov et al., 2000; Ohno et al., 2008; Underwood et al., 2005; Warzecha et al., 2009), but tissues contain numerous cell types and regulation at this level does not address how cell-type-specific alternative splicing is achieved.

In *Drosophila*, Dscam2 is a cell recognition molecule that mediates self- and cell-type-specific avoidance (tiling) (Millard et al., 2007; Millard et al., 2010). Mutually exclusive alternative splicing of exon 10A or 10B produces two isoforms with

biochemically unique extracellular domains (Millard et al., 2007). Previously, we found that the splicing of *Dscam2* is cell-type-specific (Lah et al., 2014). This deterministic splicing is crucial for the proper development of axon terminal size, dendrite morphology and synaptic numbers (Kerwin et al., 2018; Lah et al., 2014; Li et al., 2015). Although the functional consequences of disrupting regulated *Dscam2* alternative splicing have been demonstrated, what regulates this process remained unclear. Here, we conducted an RNAi screen and identified *muscleblind* (*mbl*) as a regulator of *Dscam2* alternative splicing. Loss-of-function (LOF) and overexpression (OE) studies suggest that Mbl acts both as a splicing repressor of *Dscam2* exon 10A and as an activator of exon 10B (hereafter *Dscam2.10A* and *Dscam2.10B*). Consistent with this finding, *mbl* expression is cell-type-specific and correlates with the expression of *Dscam2.10B*. Driving mbl in mushroom body neurons that normally select isoform A, induces the expression of isoform B and generates a phenotype similar to that observed in animals that express a single isoform of *Dscam2*. Although the *mbl* gene is itself alternatively spliced, we found that selection of *Dscam2.10B* does not require a specific Mbl isoform and that human MBNL1 can also regulate *Dscam2* alternative splicing. Our study demonstrates that mutually exclusive splicing of *Dscam2* is regulated by the cell-type-specific expression of a highly conserved RNA binding protein, Mbl.

72 **Results**

73 **An RNAi screen identifies *mbl* as a repressor of *Dscam2* exon 10A selection**

74 We reasoned that the neuronal cell-type-specific alternative splicing of *Dscam2* is
75 likely regulated by RNA binding proteins, and that we could identify these regulators
76 by knocking them down in a genetic background containing an isoform reporter. In
77 photoreceptors (R cells) of third instar larvae, *Dscam2.10B* is selected whereas the
78 splicing of *Dscam2.10A* is repressed (Lah et al., 2014; Tadros et al., 2016). Given that
79 quantifying a reduction in *Dscam2.10B* isoform reporter levels is challenging
80 compared to detecting the appearance of *Dscam2.10A* in cells where it is not normally
81 expressed, we performed a screen for repressors of isoform A in R cells.

82

83 To knock down RNA binding proteins, the *glass* multimer reporter (*GMR)-GAL4* was
84 used to drive RNAi transgenes selectively in R cells. Our genetic background
85 included *UAS-Dcr-2* to increase RNAi efficiency (Dietzl et al., 2007) and *GMR-GFP*
86 to mark the photoreceptors independent of the *Gal4/UAS* system (Brand and
87 Perrimon, 1993). Lastly, a *Dscam2.10A-LexA* reporter driving *LexAOp*-myristolated
88 tdTomato (hereafter *Dscam2.10A>tdTom*; Fig. 1A) was used to visualize isoform A
89 expression (Lai and Lee, 2006; Tadros et al., 2016). As expected,
90 *Dscam2.10B>tdTom* was detected in R cell projections in the lamina plexus as well as
91 in their cell bodies in the eye-disc, whereas *Dscam2.10A>tdTom* was not (Fig. 1C-
92 1D). Overexpression of Dcr-2 in R cells did not perturb the repression of
93 *Dscam2.10A* (Fig 1O). We knocked down ~160 genes using ~250 RNAi lines (Fig 1B
94 and Table S1) and identified two independent RNAi lines targeting *mbl* that caused
95 aberrant expression of *Dscam2.10A* in R cells where it is normally absent (Fig 1F,
96 1O). The penetrance increased when animals were reared at a higher temperature of

97 29°C, which is more favorable for Gal4 (Mondal et al., 2007; Ni et al., 2008) (Fig
98 1O).
99
100 Mbl-family proteins possess evolutionarily conserved tandem CCCH zinc-finger
101 domains through which they bind pre-mRNA. Vertebrate Mbl family members are
102 involved in tissue-specific splicing and have been implicated in myotonic dystrophy
103 (Pascual et al., 2006). Formerly known as *mindmelt*, *Drosophila mbl* was first
104 identified in a second chromosome *P*-element genetic screen for embryonic defects in
105 the peripheral nervous system (Kania et al., 1995). *Mbl* produces multiple isoforms
106 through alternative splicing (Begemann et al., 1997; Irion, 2012), and its function has
107 been most extensively characterized in fly muscles where both hypomorphic
108 mutations and sequestration of the protein by repeated CUG sequences within an
109 mRNA lead to muscle defects (Artero et al., 1998; Llamusi et al., 2013). To validate
110 the RNAi phenotype, we tested *Dscam2.10A>tdTom* expression in *mbl* loss-of-
111 function (LOF) mutants. Since *mbl* LOF results in lethality, we first conducted
112 complementation tests on six *mbl* mutant alleles to identify viable hypomorphic
113 combinations. These included two alleles created previously via imprecise *P*-element
114 excision (mbl^{e127} and mbl^{e27}; Begemann et al. 1997) two MiMIC splicing traps
115 ($mbl^{MI00976}$ and $mbl^{MI04093}$; (Venken et al., 2011) and two 2nd chromosome deficiencies
116 (*Df(2R)BSC154* and *Df(2R)Exel6066*; Fig 1F-1G). Consistent with previous reports,
117 the complementation tests confirmed that the majority of the alleles were lethal over
118 one another (Fig 1G) (Kania et al., 1995). However, we identified two *mbl*
119 transheterozygous combinations that were partially viable and crossed these into a
120 *Dscam2.10A>tdTom* reporter background. Both $mbl^{e127}/mbl^{MI00976}$ and
121 $mbl^{MI04093}/mbl^{MI00976}$ animals presented aberrant *Dscam2.10A* expression in R cells

122 when compared to heterozygous and wild-type controls (Fig 1H-O). *Mbl* mutant
123 mosaic clones also exhibited aberrant *Dscam2.10A>tdTom* expression in R cells (Fig
124 S1A-S1F). The weakest allele, mbl^{M00976}, which removes only a proportion of the *mbl*
125 isoforms, was the only exception (Fig S1E-S1F).
126
127 One alternative explanation of how *Dscam2.10A>tdTom* expression could get
128 switched-on in *mbl* mutants, is through exon 10 skipping. Removing both alternative
129 exons simultaneously does not result in a frameshift mutation, and since the Gal4 in
130 our reporters is inserted directly downstream of the variable exons (in exon 11), it
131 would still be expressed. To test this possibility, we amplified *Dscam2* sequences
132 between exon 9 and 11 in $mbl^{e127}/mbl^{MI00976}$ transheterozygous animals using RT-PCR.
133 In both control and *mbl* LOF mutants, we detected RT-PCR products (~690bp) that
134 corresponded to the inclusion of exon 10 (A or B) and failed to detect products
135 (~390bp) that would result from exon 10 skipping (Fig 1P). This suggested that Mbl
136 is not involved in the splicing fidelity of *Dscam2.10* but rather in the selective mutual
137 exclusion of its two isoforms. To assess whether the ratios of the two isoforms were
138 changing in the *mbl* hypomorphic mutants, we cut the exon 10 RT-PCR products with
139 the *ClaI* restriction enzyme that only recognizes exon 10A. Densitometric analysis
140 then allowed us to semi-quantitatively compare the relative levels of both isoforms.
141 There was ~25% increase in the level of exon 10A inclusion in $mbl^{e127}/mbl^{MI00976}$
142 animals compared to controls (Fig 1P), consistent with the derepression we observed
143 in our 10A reporter lines. To determine whether Mbl was specifically regulating
144 *Dscam2* exon 10 mutually exclusive splicing, we assessed other *Dscam2* alternative
145 splicing events. These included an alternative 5' splice site selection of *Dscam2* exon
146 19 and the alternative last exon (ALE) selection of exon 20 (Fig S2A). The expression

147 of these different isoforms was unchanged in *mbl* hypomorphic mutants (Fig S2B).
148 Together, our results indicate that Mbl is an essential splicing factor that specifically
149 represses *Dscam2.10A*.
150
151 **_Mbl_ is necessary for the selection of _Dscam2_ exon 10B**
152 Since *Dscam2* exon 10 isoforms are mutually exclusively spliced, we predicted that
153 selection of exon 10A would lead to the loss of exon 10B selection. To test this, we
154 conducted mosaic analysis with a repressible cell marker (MARCM) (Lee and Luo,
155 1999) to analyse *Dscam2.10B* expression in *mbl* mutant clones. In late third instar
156 brains, clones homozygous (GFP-positive) for mbl^{E127} and mbl^{E27} exhibited a dramatic
157 reduction in *Dscam2.10B>tdTom* expression in R cell axons projecting to the lamina
158 plexus compared to controls (Fig 2B, C, E). The absence of *Dscam2.10B>tdTom* in
159 *mbl* mutant clones was more striking during pupal stages (Fig 2D), suggesting that
160 perdurance of Mbl could explain the residual signal observed in third instar animals.
161 These results reveal that *mbl* is cell-autonomously required for the selection of the
162 *Dscam2.10B* isoform.
163
164 **Cell-type-specific _mbl_ expression is transcriptionally regulated**
165 Previous studies have reported that *mbl* is expressed in third instar eye-discs and
166 muscles (Artero et al., 1998; Brouwer et al., 1997). Since *mbl* LOF results in both the
167 production of *Dscam2.10A* and the loss of *Dscam2.10B*, we predicted that *mbl*
168 expression would correlate with the presence of isoform B. To test this, we
169 characterized several *mbl* reporters (Fig S3A). We analyzed three enhancer trap
170 strains (transcriptional reporters) inserted near the beginning of the *mbl* gene
171 (mbl^{k01212}-*LacZ*, mbl^{NP1161}-*Gal4* and mbl^{NP0420}-*Gal4*), as well as a splicing trap line

172 generated by the Trojan-mediated conversion of a *mbl* MiMIC (Minos Mediated
173 Integration Cassette) insertion (Fig S2A, *mbl*^{MiMIC00139}*-Gal4;* (Diao et al., 2015). The
174 splicing trap reporter consists of a splice acceptor site and an in-frame *T2A-Gal4*
175 sequence inserted in an intron between two coding exons. This *Gal4* cassette gets
176 incorporated into *mbl* mRNA during splicing and therefore Gal4 is only present when
177 *mbl* is translated. Consistent with previous studies, and its role in repressing the
178 production of *Dscam2.10A*, all four *mbl* reporters were expressed in the third instar
179 photoreceptors (Fig 3A, S3A-S3B and data not shown). We next did a more
180 extensive characterization of *mbl* expression by driving nuclear localized GFP
181 (*GFP.nls*) with one transcriptional (*mbl*^{NP0420}*-Gal4)* and one translational
182 (*mbl*^{MiMIC00139}*-Gal4)* reporter. In the brain, we found that *mbl* was expressed
183 predominantly in postmitotic neurons with some expression detected in glial cells (Fig
184 S3C-S3F and S3H-S3K). Interestingly, we detected the translational but not the
185 transcriptional reporter in third instar muscles (Fig S3G and S3L). The absence of
186 expression is likely due to the insertion of the *P*-element into a neural-specific
187 enhancer, as previously described (Bargiela et al., 2014). To assess the expression of
188 *mbl* in the five lamina neurons L1- L5, all of which express *Dscam2* (Lah et al., 2014;
189 Tadros et al., 2016), we implemented an intersectional strategy using a
190 *UAS>stop>epitope* reporter (Nern et al., 2015) that is dependent on both *FLP* and
191 *Gal4*. The *FLP* source (*Dac-FLP*) was expressed in lamina neurons and able to
192 remove the transcriptional stop motif in the reporter transgene. The overlap between
193 *mbl-Gal4* and *Dac-FLP* allowed us to visualize *mbl* expression in lamina neurons at
194 single-cell resolution (Fig 3B). As a proof of principle, we first did an intersectional
195 analysis with a pan-neuronal reporter, *elav-Gal4* (Fig 3C$_1$). We detected many clones
196 encompassing various neuronal-cell-types including the axons of L1-L5 and R7-R8

197 (Fig 3C-3D). This confirmed that all lamina neurons could be detected using this
198 strategy. Using *mbl-Gal4* reporters we found that L1, which expresses *Dscam2.10B*,
199 was the primary neuron labelled. A few L4 cells were also identified, which is
200 consistent with this neuron expressing *Dscam2.10B* early in development and
201 *Dscam2.10A* at later stages (Tadros et al., 2016). To confirm this finding, we
202 dissected the expression of *mbl* in lamina neurons during development. Using the
203 same intersectional strategy, we detected a high number of L4 clones at 48hr apf
204 (30%, n=10). This was followed by a decline at 60hr apf (26.7%, n = 30) and 72hr apf
205 (11.8%, n = 85) reaching the lowest at eclosion (Fig S4A and S4B;1.7%, n=242).
206 Thus, *mbl* expression in L4 neurons mirrors the expression of *Dscam2.10B*.
207 Consistent with this, L2, L3 and L5, were all detected using the intersectional strategy
208 with *Dscam2.10A-Gal4* but were not labelled using *mbl-Gal4* (Fig 3E). Together,
209 these results show that cell-type-specific *mbl* expression is transcriptionally regulated
210 and correlates with the cell-type-specific alternative splicing of *Dscam2*. Cells that
211 select *Dscam2.10B* and repress *Dscam2.10A* express *mbl*. In contrast, *mbl* was not
212 detected in cells that repress *Dscam2.10B* and select *Dscam2.10A*.
213
214 **Ectopic expression of multiple *mbl* isoforms are sufficient to promote the**
215 **selection of *Dscam2* exon 10B**
216 Our analysis in the visual system demonstrated that *mbl* is necessary for the selection
217 of *Dscam2.10B*, but we wondered whether it was sufficient to promote exon 10B
218 selection in cell types that normally repress this isoform. To test this possibility, we
219 overexpressed *mbl* ubiquitously and monitored isoform B expression using
220 *Dscam2.10B>tdTom*. We focussed on the mushroom body (MB), as this tissue
221 expresses isoform A specifically in α'β' neurons at 24hr apf where mbl is not

222 detected (Fig 3G-3H, 4A-4C). Consistent with *mbl* being sufficient for isoform B
223 selection, ubiquitous expression of *mbl* using an enhancer trap containing a *UAS*
224 insertion at the 5' end of the gene (*Act5c>mbl*$^{B2\text{-}E1}$), switched on *Dscam2.10B* in α'β'
225 MB neurons, where it is normally absent (Fig 4D). Ectopic *mbl* expression in MB
226 neurons with *OK107-Gal4* also led to selection of *Dscam2.10B* expression
227 specifically in α'β' neurons at 24-36hr apf. Although our two *Gal4* drivers expressed
228 *mbl* in all MB neurons, *Dscam2.10B* was only observed in α'β' neurons,
229 demonstrating that transcription of *Dscam2* is a pre-requisite for this splicing
230 modulation. Previous studies have suggested that the *mbl* gene is capable of
231 generating different isoforms with unique functions depending on their subcellular
232 localization (Vicente et al., 2007). This also includes the production of a highly
233 abundant circular RNA that can sequester the Mbl protein (Ashwal-Fluss et al., 2014;
234 Houseley et al., 2006). To assess whether *Dscam2* exon 10B selection is dependent on
235 a specific alternative variant of Mbl, we overexpressed the cDNAs of fly *mbl*
236 isoforms (*mblA*, *mblB* and *mblC*; (Begemann et al., 1997; Juni and Yamamoto, 2009)
237 as well as an isoform of the human *MBNL1* that lacks the linker region optimal for
238 CUG repeat binding (*MBNL1*$_{35}$; (Kino et al., 2004; Li et al., 2008) with either *Act5c-*
239 *Gal4* or *OK107-Gal4*. These constructs all possess the tandem N-terminal CCCH
240 motif that binds to YCGY sequences and lack the ability to produce *mbl* circRNA. In
241 all cases, overexpression resulted in the misexpression of *Dscam2.10B* in α'β' MBs
242 (with the exception *Act5C>mblC*, which resulted in lethality; Fig 4D-4E). Using
243 semi-quantitative RT-PCR from the *Act5C>mbl* flies, we demonstrated that
244 overexpression of *mbl* did not lead to exon 10 skipping and that it increased exon 10B
245 selection by 8-24% (Fig 4F), depending on the *mbl* isoform used. The inability of Mbl
246 to completely inhibit exon 10A selection suggests that other factors or mechanisms

247 may also contribute to cell-specific *Dscam2* isoform expression (see Discussion).
248 These results suggest that Mbl protein isoforms are all capable of *Dscam2.10B*
249 selection and independent of *mbl* circRNA. The ability of human MBNL1 to promote
250 the selection of exon 10B suggests that the regulatory logic for *Dscam2* splicing is
251 likely conserved in other mutually-exclusive cassettes in higher organisms.
252
253 Finally, we observed a phenotype in MB neurons overexpressing *mbl* where the β
254 lobe neurons inappropriately crossed the midline (Fig 4G-4I). Interestingly, a similar
255 phenotype was observed in flies expressing a single isoform of *Dscam2* that we
256 previously generated using recombinase-mediated cassette exchange (Lah et al.,
257 2014). These flies express a single isoform in all *Dscam2* positive cells. We
258 quantified this phenotype and found that the *Dscam2A*, but not the *Dscam2B*, single
259 isoform line generated a MB fusion phenotype that was significantly different from
260 controls. All of the *UAS-mbl* constructs, except human *MBNL1*, generated this
261 phenotype at a penetrance that was equal to or greater than *Dscam2A* single isoform
262 lines (Fig 4I). The lack of a phenotype with the human transgene is consistent with
263 this modified isoform having a reduced CUG-binding capacity due to its missing
264 linker domain (Kino et al., 2004; Li et al., 2008). These data demonstrate that MB
265 phenotypes generated in animals overexpressing *mbl*, phenocopy *Dscam2* single
266 isoform mutants. While the origin of this non-autonomous phenotype is not known, it
267 correlates with the misregulation of *Dscam2* alternative isoform expression.
268
269 **Discussion**
270 In this study, we identify Mbl as a regulator of *Dscam2* alternative splicing. We
271 demonstrate that removing *mbl* in a *mbl*-positive cell-type results in a switch from

272 *Dscam2.10B* to *Dscam2.10A* selection. Ectopic expression of a variety of Mbl protein
273 isoforms in a normally *mbl*-negative neuronal cell-type is sufficient to trigger the
274 selection of *Dscam2.10B*. Consistent with this, transcriptional reporters demonstrate
275 that *mbl* is expressed in a cell-type-specific manner, which tightly correlates with
276 *Dscam2.10B*. Lastly, misexpression of *mbl* leads to a MB phenotype that is also
277 observed in flies that express a single *Dscam2* isoform.
278
279 One surprising finding in this study was that *mbl* expression itself is regulated in a
280 cell-specific manner. *Mbl* was present in all cells tested that express *Dscam2.10B* and
281 absent from *Dscam2.10A* cells. Mbl appears to be regulated at the transcriptional level
282 since enhancer-trap as well as splicing-trap reporters exhibit similar expression
283 patterns (Fig 3). This was unexpected as 1) examples of cell-specific expression of
284 splicing factors are rare in the literature and 2) *mbl* encodes numerous alternative
285 isoforms that could be individually post-transcriptionally regulated, thus bypassing
286 the need for transcriptional control of the gene. It will be interesting to explore the *in*
287 *vivo* expression patterns of other splicing factors to determine whether cell-specific
288 expression of a subset of splicing factors is a common mechanism for regulating
289 alternative splicing in the brain.
290
291 Given that Mbl can repress exon 10A and select exon 10B (Fig 4J), it is possible that
292 this single splicing factor and its associated co-factors are sufficient to regulate
293 *Dscam2* cell-specific isoform expression. It could be that *Dscam2.10A* is the default
294 exon selected when the Mbl complex is not present. In this way, cells that express
295 *Dscam2* would be '10A' positive if they did not express *mbl* and '10B' positive if
296 they did. The observation that *Dscam2* is not expressed in all neurons and our RT-

297 PCR data, however, argue that *Dscam2* mutually exclusive alternative splicing may
298 be more complicated than this model. In MB α'β' neurons, which select exon 10A,
299 ectopic expression of *mbl* using *Act5C-Gal4* can switch on a *Dscam2.10B>tdTom*
300 reporter, but the change in isoform expression in the whole brain as measured by RT-
301 PCR is only 8-24% (see Fig 4F). One might expect a much more dramatic shift to
302 isoform B if Mbl were the only regulator/mechanism involved. In addition, if
303 *Dscam2.10A* were expressed by default in the absence of *mbl*, we would expect all
304 MB neurons to express this isoform, but this is not the case. Further studies, including
305 screens for repressors or activators of exon 10B, will be required to resolve this issue.
306
307 The MB midline crossing phenotype that is generated through both the ectopic
308 expression of *mbl* and *Dscam2A* single isoform lines supports the idea that this
309 phenotype arises from a disruption in *Dscam2* cell-specific isoform expression.
310 However, since both single isoform lines have identical expression patterns
311 (expressed in all *Dscam2*-positive cells), one would expect both lines to exhibit the
312 midline crossing phenotype if it is caused by inappropriate homophilic interactions
313 between cells that normally express different isoforms. Although there is a trend
314 towards increased fusion in animals expressing only Dscam2B (Fig 4I), it did not
315 reach statistical significance. This issue may have to do with innate differences
316 between isoform A and isoform B that are not completely understood. It is possible
317 that isoform A and B are not identical in terms of signalling due to either differences
318 in homophilic binding or differences in co-factors associated with specific isoforms.
319 Consistent with this notion, we previously reported that *Dscam2A* lines produce
320 stronger phenotypes at photoreceptor synapses compared to *Dscam2B*. Another
321 perplexing aspect about the MB phenotype is that it occurs in neurons that either do

322 not express *Dscam2* (β lobe neurons) or express it at such low levels that it is not
323 detectable with our reporters. Thus, the phenotype must arise indirectly. This could
324 occur through inappropriate interactions between α'β' neurons and another non-MB
325 cell type within this brain region that expresses *Dscam2*. Alternatively, this phenotype
326 could be independent of Dscam2 homophilic binding and instead reflect differences in
327 isoform complexes that form in different neurons.
328
329 How does Mbl repress *Dscam2.10*A and select *Dscam2.10B* at the level of pre-
330 mRNA? The vertebrate orthologue of Mbl, MBNL1 binds to YCGY (where Y is a
331 pyrimidine) in pre-mRNAs and untranslated regions using its tandem zinc-finger
332 domains, but it is quite promiscuous (Wang et al., 2012). The best-characterised
333 alternative splicing events regulated by MBNL1 are exon skipping or inclusion
334 events. In general, an exon that contains MBNL1 binding sites upstream or within the
335 coding sequence is subject to skipping, whereas downstream binding sites more often
336 promote inclusion (reviewed in Konieczny et al 2014). The mechanisms used by fly
337 Mbl to regulate splicing have not been characterised in detail, but given that human
338 MBNL1 can rescue fly *mbl* lethality and promote the endogenous expression of
339 *Dscam2* exon 10B in MBs, presumably the mechanisms are conserved. A simple
340 explanation for how Mbl regulates *Dscam2* mutually exclusive splicing would be that
341 it binds upstream of exon 10A to repress exon inclusion and downstream of exon 10B
342 to promote inclusion. Although there are many potential binding sites for Mbl
343 upstream, downstream and within the alternative exons, an obvious correlation
344 between location and repression vs inclusion is not observed. There is also a large
345 (3kb) intron downstream of exon 10B that could contain *cis* regulatory elements.
346 Identification of the sequences required for regulation by Mbl will therefore require

347 extensive mapping and ultimately validation using a technique like cross-linking
348 followed by immunoprecipitation (CLIP).
349
350 Together, our results demonstrate that selective expression of a splicing factor can
351 drive neuronal cell-type specific alternative splicing. These data provide clues into
352 how the brain can diversify its repertoire of proteins that promote neural connectivity.
353 It is likely that Mbl is regulating the alternative splicing of other developmental genes
354 in concert with *Dscam2* and therefore regulated splicing factors such as Mbl may
355 represent hubs of neurodevelopment.
356
357 **Experimental procedures**
358 **Fly strains**
359 *Dscam2.10A-LexA* and *Dscam2.10B-LexA* (Tadros et al., 2016), *UAS-Dcr2* and *UAS-*
360 *mbl-RNAi*^{VDRC28732} (Dietzl et al., 2007), *LexAop-myr-tdTomato* (attP2, (Chen et al.,
361 2014), *UAS-Srp54-RNAi*$^{TRiP.HMS03941}$, *CadN-RNAi*$^{TRiP.HMS02380}$ and *UAS-mbl-*
362 *RNAi*$^{TRiP.JF03264}$(Ni et al., 2008), *UAS-mCD8-GFP* (Lee and Luo, 1999), *FRT42D* (Xu
363 and Rubin, 1993), *mbl*^{e127} and *mbl*^{e27}(Begemann et al., 1997), *mbl*^{MI00976} and *mbl*^{MI04093}
364 (Venken et al., 2011), *Df(2R)BSC154* (Cook et al., 2012), *Df(2R)Exel6066* (Parks et
365 al., 2004), *ey-FLP* (Chr.1, (Newsome et al., 2000), *GMR-myr-GFP*, *mbl*^{NP0420}*-Gal4*
366 and *mbl*^{NP1161}*-Gal4* (Hayashi et al., 2002), *mbl*^{k01212}*-LacZ* (Spradling et al., 1999),
367 *mbl*^{MiMIC00139}*-Gal4* (H. Bellen Lab), *Dac-FLP* (Chr.3, (Millard et al., 2007),
368 *UAS>stop>myr::smGdP-V5-THS-UAS>stop>myr::smGdP-cMyc* (attP5, (Nern et al.,
369 2015), *Dscam2.10A-Gal4* and *Dscam2.10B-Gal4* (Lah et al., 2014) *Act5C-Gal4*
370 (Chr.3, from Yash Hiromi), *OK107-Gal4* (Connolly et al., 1996), *UAS-mblA*, *UAS-*

371 *mblB* and *UAS-mblC* (D. Yamamoto Lab), *P{EP}mbl*$^{B2\text{-}E1}$, *UAS-mblA-FLAG* and

372 *UAS-MBNL1*$_{35}$ (Li et al., 2008).

373

374 **RNAi screening**

375 The RNAi screen line was generated as follows: *GMR-Gal4* was recombined with

376 *GMR-GFP* on the second chromosome. *Dscam2.10A-LexA* (Tadros et al. 2016) was

377 recombined with *LexAop-myr-tdTomato* on the third chromosome. These flies were

378 crossed together with *UAS-Dcr-2* (X) to make a stable RNAi screen stock. Virgin

379 females were collected from this RNAi screen stock, crossed to UAS-RNAi males

380 and reared at 25°C. Wandering third instar larvae were dissected and fixed. We tested

381 between one and three independent RNAi lines per gene. Brains were imaged without

382 antibodies using confocal microscopy. RNAi lines tested are listed in Table S1.

383

384 **Semiquantitative RT-PCR**

385 Total RNA was isolated using TRIzol (Ambion) following the manufacturer's

386 protocol. Reverse transcription was performed on each RNA sample with random

387 primer mix using 200 units of M-MULV (NEB) and 2 μ g of RNA in a 20 μ l

388 reaction, at 42°C for 1 hr. PCR reactions were set up with specific primers to analyse

389 alternative splicing of various regions of *Dscam2*. Where possible, semi-quantitative

390 PCR was performed to generate multiple isoforms in a single reaction and relative

391 levels were compared by electrophoresis.

392

393 **Immunohistochemistry**

394 Immunostaining were conducted as previously described (Lah et al. 2014). Antibody

395 dilutions used were as follows: mouse mAb24B10 (1:20; DSHB), mouse anti-Repo

396 (1:20; DSHB), mout anti-DAC (1:20; DSHB), mouse anti-Fas2 (1:20; DSHB) rat
397 anti-ELAV (1:200), V5-tag:DyLight anti-mouse 550 (1:500; AbD Serotec), V5-
398 tag:DyLight anti-mouse 405 (1:200; AbD Serotec), myc-tag;DyLight anti-mouse 549
399 (1:200; AbD Serotec), Phalloidin:Alexa Fluor 568 (1:200; Molecular Probes),
400 DyLight anti-mouse 647 (1:2000; Jackson Laboratory), DyLight Cy3 anti-rat (1:2000;
401 Jackson Laboratory).
402
403 **Image acquisition**
404 Imaging was performed at the School of Biomedical Sciences Imaging Facility.
405 Images were taken on a Leica SP8 laser scanning confocal system with a 63X
406 Glycerol NA 1.3.
407
408 **Fly genotypes**
409 <u>R cell RNAi experiments (Figure 1)</u>
410 *w; GMR-GFP, GMR-Gal4/CyO; Dscam2.10B-LexA, LexAop-myr-tdTomato/TM6B*
411 *w; GMR-GFP, GMR-Gal4/CyO; Dscam2.10A-LexA, LexAop-myr-tdTomato/TM6B*
412 *w, UAS-Dcr-2; GMR-GFP, GMR-Gal4/CyO; Dscam2.10A-LexA, LexAop-myr-*
413 *tdTomato/TM6B*
414 *w, UAS-Dcr-2; GMR-GFP, GMR-Gal4/UAS-mCD8-RFP; Dscam2.10A-LexA,*
415 *LexAop-myr-tdTomato/+*
416 *w, UAS-Dcr-2; GMR-GFP, GMR-Gal4/UAS-mbl-RNAi(v28732); Dscam2.10A-LexA,*
417 *LexAop-myr-tdTomato/+*
418 *w, UAS-Dcr-2; GMR-GFP, GMR-Gal4/+; Dscam2.10A-LexA, LexAop-myr-*
419 *tdTomato/UAS-mbl-RNAi(TRiP.JF03264)*
420

421 <u>mbl whole animal experiments (Figure 1)</u>

422 *w; +; Dscam2.10B-LexA, LexAop-myr-tdTomato/TM6B*

423 *w; +; Dscam2.10A-LexA, LexAop-myr-tdTomato/TM6B*

424 *w; mbl^{e127}/CyO,GFP; Dscam2.10A-LexA, LexAop-myr-tdTomato/TM6B*

425 *w; mbl^{MI00976}/CyO,GFP; Dscam2.10A-LexA, LexAop-myr-tdTomato/TM6B*

426 *w; mbl^{MI04093}/CyO,GFP; Dscam2.10A-LexA, LexAop-myr-tdTomato/TM6B*

427 *w; mbl^{e127}/ mbl^{MI00976}; Dscam2.10A-LexA, LexAop-myr-tdTomato/+*

428 *w; mbl^{MI04093}/ mbl^{MI00976}; Dscam2.10A-LexA, LexAop-myr-tdTomato/+*

429

430 <u>mbl ey-FLP mosaic experiments (Figure 1)</u>

431 *w, ey-FLP; FRT42D, GMR-myr-GFP/FRT42D; Dscam2.10B-LexA, LexAop-myr-*

432 *tdTomato, UAS-mCD8-GFP/+*

433 *w, ey-FLP; FRT42D, GMR-myr-GFP/FRT42D; Dscam2.10A-LexA, LexAop-myr-*

434 *tdTomato, UAS-mCD8-GFP/+*

435 *w, ey-FLP; FRT42D, GMR-myr-GFP/FRT42D, Df(2R)154 ; Dscam2.10A-LexA,*

436 *LexAop-myr-tdTomato, UAS-mCD8-GFP/+*

437 *w, ey-FLP; FRT42D, GMR-myr-GFP/FRT42D, mbl^{e27}; Dscam2.10A-LexA, LexAop-*

438 *myr-tdTomato, UAS-mCD8-GFP/+*

439 *w, ey-FLP; FRT42D, GMR-myr-GFP/FRT42D, mbl^{MI00976}; Dscam2.10A-LexA,*

440 *LexAop-myr-tdTomato, UAS-mCD8-GFP/+*

441

442 <u>mbl ey-FLP MARCM experiments (Figure 3)</u>

443 *w, ey-FLP; FRT42D, Tub-Gal80/FRT42D; Dscam2.10A-LexA, LexAop-myr-*

444 *tdTomato, Act5c-Gal4, UAS-mCD8-GFP/+*

445 *w, ey-FLP; FRT42D, Tub-Gal80/FRT42D, mbl^{e27}; Dscam2.10A-LexA, LexAop-myr-*

446 *tdTomato, Act5c-Gal4, UAS-mCD8-GFP/+*

447 *w, ey-FLP; FRT42D, Tub-Gal80/FRT42D, mbl^{e127}; Dscam2.10A-LexA, LexAop-myr-*

448 *tdTomato, Act5c-Gal4, UAS-mCD8-GFP/+*

449

450 <u>mbl expression experiments (Figure 3)</u>

451 *w; UAS-mCD8-GFP/+; mbl^{NP0420}-Gal4/+*

452 *w; UAS-mCD8-GFP/+; mbl^{MI00139}-Gal4/+*

453 *w; Dac-FLP/+; elav-Gal4/ UAS>stop>myr::smGdP-V5-THS-*

454 *UAS>stop>myr::smGdP-cMyc*

455 *w; Dac-FLP/+; mbl^{NP0420}-Gal4/ UAS>stop>myr::smGdP-V5-THS-*

456 *UAS>stop>myr::smGdP-cMyc*

457 *w; Dac-FLP/+; mbl^{MI00139}-Gal4/ UAS>stop>myr::smGdP-V5-THS-*

458 *UAS>stop>myr::smGdP-cMyc*

459 *w; Dac-FLP/+; Dscam2.10A-Gal4/ UAS>stop>myr::smGdP-V5-THS-*

460 *UAS>stop>myr::smGdP-cMyc*

461 *w; Dac-FLP/+; Dscam2.10B-Gal4/ UAS>stop>myr::smGdP-V5-THS-*

462 *UAS>stop>myr::smGdP-cMyc*

463 *w; +; mbl^{NP0420}-Gal4/UAS-GFP.nls*

464 *w; +; mbl^{MI00139}-Gal4/UAS-GFP.nls*

465

466 <u>mbl ectopic expression in MBs (Figure 4)</u>

467 *w; +; Dscam2.10A-LexA, LexAop-myr-tdTomato, Act5c-Gal4, UAS-mCD8-GFP/+*

468 *w; +; Dscam2.10B-LexA, LexAop-myr-tdTomato, Act5c-Gal4, UAS-mCD8-GFP/+*

469 *w; P{EP}mbl^{B2-E1}/+; Dscam2.10B-LexA, LexAop-myr-tdTomato, Act5c-Gal4, UAS-*

470 *mCD8-GFP/+*

471 *w; +; Dscam2.10B-LexA, LexAop-myr-tdTomato, Act5c-Gal4, UAS-mCD8-*

472 *GFP/UAS-mblA*

473 *w; +; Dscam2.10B-LexA, LexAop-myr-tdTomato, Act5c-Gal4, UAS-mCD8-*

474 *GFP/UAS-mblB*

475 *w; +; Dscam2.10B-LexA, LexAop-myr-tdTomato, Act5c-Gal4, UAS-mCD8-*

476 *GFP/UAS-mblC*

477 *w; +; Dscam2.10B-LexA, LexAop-myr-tdTomato, Act5c-Gal4,UAS-mCD8-GFP/UAS-*

478 *MBNL1$_{35}$*

479 *w; +; Dscam2.10B-LexA, LexAop-myr-tdTomato, UAS-mCD8-GFP/UAS-mblA;*

480 *OK107-Gal4/+*

481 *w; +; Dscam2.10B-LexA, LexAop-myr-tdTomato, UAS-mCD8-GFP/UAS-mblB;*

482 *OK107-Gal4/+*

483 *w; +; Dscam2.10B-LexA, LexAop-myr-tdTomato, UAS-mCD8-GFP/UAS-mblC;*

484 *OK107-Gal4/+*

485 *w; +; Dscam2.10B-LexA, LexAop-myr-tdTomato, UAS-mCD8-GFP/UAS-MBNL1$_{35}$;*

486 *OK107-Gal4/+*

487

488

489 **Author contribution**

490 J.S.S.L designed and performed all experiments. S.S.M supervised the project. J.S.S.L

491 and S.S.M wrote the manuscript.

492

493 **Acknowledgements**

494 We thank Wael Tadros, Larry Zipursky, Greg Neely, Louis O'Keefe, Nancy Bonini,
495 Aljoscha Nern and Bloomington Stock Center for sharing fly stocks. We thank the
496 Daisuke Yamamoto Lab for constructing the *UAS-mbl* lines deposited and maintained
497 at the Kyoto Stock Center. We thank Shaun Walters for technical assistance on the
498 Leica confocal microscopy. We thank Kevin Mutemi for characterizing Dscam2
499 isoform expression in mushroom bodies and all midline crossing defects in Dscam2
500 single isoform mutant animals. We thank Grace Shin for her initial characterization of
501 *Dscam2* isoform expression in adults and Wei Jun Tan for triple balancing *OK107-*
502 *Gal4*. We also thank members of the Millard, Pecot, Hilliard and van Swinderen lab
503 for their feedback. The RNAi screen was inspired by the works of Hidehito
504 Kuroyanagi. This work was supported by the National Health and Medical Research
505 Council of Australia (NHMRC grant APP1021006). J.S.S.L was supported by the
506 Australia Postgraduate Award (Research Training Scheme) from the Australian
507 Federal Government.
508

509 **Figure legends**

510 **Figure 1.** *Drosophila mbl* is required for the repression of *Dscam2* exon 10A in R
511 cells. (A) Schematic showing the region of *Dscam2* exon 10 that undergoes mutually
512 exclusive alternative splicing and the LexA isoform-specific reporter lines. Frame-
513 shift mutations in the exon not reported are shown. (B) Schematic RNAi screen
514 design for identifying repressors of *Dscam2* exon 10A selection. R cells normally
515 select exon 10B and repress exon 10A. We knocked-down RNA binding proteins in R
516 cells while monitoring 10A expression.
517 (C-E) *Dscam2* exon 10A is derepressed in R cells when mbl is knocked-down. (C_1-
518 C_3) *Dscam2.10B* control. R cells (green) normally select exon 10B (red). R cell

519 terminals can be observed in the lamina plexus (angle brackets). *Dscam2.10B* is also
520 expressed in the developing optic lobe (arrowhead). (D_1-D_3) *Dscam2.10A* is not
521 expressed in R cells (green) but is expressed in the developing optic lobe (arrowhead).
522 (E_1-E_3) RNAi lines targeting *mbl* in R cells results in the aberrant expression of
523 *Dscam2.10A* in R cells.
524 (F) Schematic of the *mbl* gene showing the location of two small deletions (*E27* and
525 *E127*), two MiMIC insertions (*MI04093* and *MI00976*) and two deficiencies
526 (*Df(2R)Exel6066 and Df(2R)BSC154*) used in this study. Non-coding exons are in
527 gray, coding exons are black.
528 (G) Complementation test of *mbl* loss-of-function (LOF) alleles. Numbers in the table
529 represent the number of non-*CyO* offspring over the total. Most transheterygote
530 combinations were lethal with the exception of $mbl^{MI00976}/mbl^{e27}$ and
531 $mbl^{MI00976}/mbl^{MI04093}$ (green).
532 (H-N) *Mbl* transheterozygotes express *Dscam2.10A* in R cells. (H) *Dscam2.10B*
533 control showing expression in the lamina plexus (angle brackets). (I) *Dscam2.10A*
534 control showing no expression of this isoform in R cells. (J-L) Heterozygous animals
535 for *mbl* LOF alleles are comparable to control. (M-N) Two different *mbl*
536 transheterozygote combinations exhibit de-repression of *Dscam2.10A* in R cells.
537 (O) Quantification of *Dscam2.10>tdTom* expression in third instar R cells with
538 various *mbl* manipulations; including RNAi knockdown (black bars) and whole
539 animal transheterozygotes (white). Y-axis represents the number of optic lobes with R
540 cells positive for tdTom over total quantified as a percentage. On the x-axis, the
541 presence of a transgene is indicated with a blue box and the temperature at which the
542 crosses were reared (25°C or 29°C) is indicated.

543 (P) *Dscam2* exon 10A inclusion is increased in *mbl* transheterozygotes. (Top)
544 Semiquantitative RT-PCR from different genotypes indicated. Primers amplified the
545 variable region that includes exon 10. A smaller product that would result from exon
546 10 skipping is not observed. (Bottom) Exon 10A-specific cleavage with restriction
547 enzyme ClaI shows an increase in exon 10A inclusion in mbl transheterozygotes.
548 Percentage of exon 10A inclusion was calculated by dividing 10A by 10A+10B bands
549 following restriction digest. See also Figures S1 and S2.
550
551 **Figure 2.** *Drosophila* Mbl is necessary for the selection of *Dscam2* exon 10B in R
552 cells.
553 (A) Schematic of our predicted *mbl* MARCM results using *ey-FLP*. WT R cell clones
554 will be GFP(+) and *Dscam2.10B>tdTom*(+) (yellow), whereas *mbl* mutant clones will
555 be *Dscam2.10B>tdTom*(-) (green). (B_1-B_3) Control MARCM clones (green) in 3rd
556 instar R cells (angle brackets) are positive for *Dscam2.10B>tdTom* (arrowhead). (C_1-
557 C_3) In mbl^{e27} clones, *Dscam2.10B* labelling in the lamina plexus is discontinuous and
558 its absence correlates with the loss of Mbl (arrowhead). (D_1-D_2) *Mbl* MARCM clones
559 from midpupal optic lobes lack *Dscam2.10B*>tdTom. (E_1-E_3) A different allele
560 (mbl^{e127}) exhibits a similar phenotype in third instar brains.
561
562 **Figure 3. *Mbl* is expressed in a cell-specific manner that correlates with**
563 *Dscam2.10B*
564 (A) A *mbl* Gal4 reporter (green) is expressed in third instar R cells but not in lamina
565 neuron precursor cells labelled with an antibody against Dacshund (DAC, red).

566 (B) Schematic of MultiColor FlpOut (MCFO) approach to characterize *mbl* reporter
567 expression in lamina neurons at adult stages. The UAS FlpOut construct produces an
568 epitope-tagged version of a non-fluorescent GFP (smGFP,(Nern et al., 2015))
569 (C_1-C_4) *Mbl* can be detected in all lamina neurons using a MCFO strategy with a pan-
570 neuronal reporter (*elav-Gal4*). Lamina neurons were identified based on their unique
571 axon morphologies. (D_1-D_4) An intersectional strategy using *mbl-Gal4* labels
572 primarily L1 lamina neurons. (E) Quantification of lamina neurons and R7-R8
573 neurons observed using the intersectional strategy. Dark blue and light blue boxes
574 represent high and low numbers of labelled neurons, respectively. (F-H) *Mbl* is not
575 expressed in mushroom body (MB) neurons that express *Dscam2.10A* at 24hr apf.
576 (F_1-F_2) *Dscam2.10A* is expressed in α'β' MB neurons that are not labelled by Fas2.
577 Fas2 labels the αβ and γ subsets of MB neurons. (G-H) Neither *Dscam2.10B* (G_1-G_2)
578 nor *mbl* (H_1-H_2) are detected in MB neurons. See also Figures S3 and S4.
579
580 **Figure 4.** All fly *mbl* isoforms can select *Dscam2* exon 10B and promote a midline
581 crossing phenotype in MBs.
582 (A) Schematic showing that *mbl* is sufficient to drive *Dscam2.10B* selection in
583 α'β'neurons.
584 (B) Control showing that *Dscam2.10A* (red) is expressed in α'β' neurons at 24hr apf.
585 (C) *Dscam2.10B* is normally repressed in α'β' neurons. (D) Overexpression of *mbl*
586 activates *Dscam2.10B* selection (red) in α'β' neurons. (E) Quantification of
587 *Dscam2.10* expression in α'β' neurons at 24-36hr apf with and without *mbl* OE.
588 Ubiquitous driver (*Act5c-Gal4*, black bars) and pan-mushroom body neuron driver
589 (*OK107-Gal4*, white bars). Y-axis represents the number of tdTom positive (+) α'β'
590 over the total, expressed as a percentage. Ratio of tdTom(+)/total is shown in each

591 bar. (F) *Mbl* OE increases *Dscam2* exon 10B inclusion. Semiquantitative RT-PCR as
592 in Figure 1. Exon 10A-specific cleavage with restriction enzyme ClaI shows an
593 increase in exon 10B inclusion in *mbl* OE animals, without exon 10 skipping.
594 (G) A representative confocal image of control adult αβ lobes (red) with clear
595 separation between the two β-lobes at the midline. (H) A representative confocal
596 image of adult αβ lobes from an animal overexpressing *mblA*. β-lobe axons
597 inappropriately cross the midline (arrowhead). (I) Quantification of β-lobe axon
598 midline crossing defects. Numbers in parentheses represent total number of
599 mushroom bodies quantified. Fishers exact test was used to compare genotypes to
600 their corresponding controls (white bars). n.s (not significant) $P>0.05$, * $P<0.05$ and
601 **** $P<0.0001$. (J) Model illustrating that Mbl represses *Dscam2.10A* and selects
602 *Dscam2.10B*.
603
604
605
606

607 **References**

608 Artero, R., Prokop, A., Paricio, N., Begemann, G., Pueyo, I., Mlodzik, M., Perez-
609 Alonso, M., and Baylies, M.K. (1998). The muscleblind gene participates in the
610 organization of Z-bands and epidermal attachments of Drosophila muscles and is
611 regulated by Dmef2. Developmental biology 195, 131-143.
612 Ashwal-Fluss, R., Meyer, M., Pamudurti, N.R., Ivanov, A., Bartok, O., Hanan, M.,
613 Evantal, N., Memczak, S., Rajewsky, N., and Kadener, S. (2014). circRNA
614 biogenesis competes with pre-mRNA splicing. Molecular cell 56, 55-66.
615 Bargiela, A., Llamusi, B., Cerro-Herreros, E., and Artero, R. (2014). Two enhancers
616 control transcription of Drosophila muscleblind in the embryonic somatic
617 musculature and in the central nervous system. PloS one 9, e93125.
618 Begemann, G., Paricio, N., Artero, R., Kiss, I., Perez-Alonso, M., and Mlodzik, M.
619 (1997). muscleblind, a gene required for photoreceptor differentiation in
620 Drosophila, encodes novel nuclear Cys3His-type zinc-finger-containing proteins.
621 Development 124, 4321-4331.
622 Bell, T.J., Thaler, C., Castiglioni, A.J., Helton, T.D., and Lipscombe, D. (2004). Cell-
623 specific alternative splicing increases calcium channel current density in the pain
624 pathway. Neuron 41, 127-138.
625 Blanchette, M., Green, R.E., MacArthur, S., Brooks, A.N., Brenner, S.E., Eisen, M.B.,
626 and Rio, D.C. (2009). Genome-wide analysis of alternative pre-mRNA splicing and
627 RNA-binding specificities of the Drosophila hnRNP A/B family members.
628 Molecular cell 33, 438-449.
629 Brand, A.H., and Perrimon, N. (1993). Targeted gene expression as a means of
630 altering cell fates and generating dominant phenotypes. Development 118, 401-
631 415.
632 Brouwer, J., Nagelkerke, D., den Heijer, P., Ruiter, J.H., Mulder, H., Begemann, M.J.,
633 and Lie, K.I. (1997). Analysis of atrial sensed far-field ventricular signals: a
634 reassessment. Pacing and clinical electrophysiology : PACE 20, 916-922.
635 Calarco, J.A., Superina, S., O'Hanlon, D., Gabut, M., Raj, B., Pan, Q., Skalska, U.,
636 Clarke, L., Gelinas, D., van der Kooy, D., *et al.* (2009). Regulation of vertebrate
637 nervous system alternative splicing and development by an SR-related protein.
638 Cell 138, 898-910.
639 Chen, Y., Akin, O., Nern, A., Tsui, C.Y., Pecot, M.Y., and Zipursky, S.L. (2014). Cell-
640 type-specific labeling of synapses in vivo through synaptic tagging with
641 recombination. Neuron 81, 280-293.
642 Connolly, J.B., Roberts, I.J., Armstrong, J.D., Kaiser, K., Forte, M., Tully, T., and
643 O'Kane, C.J. (1996). Associative learning disrupted by impaired Gs signaling in
644 Drosophila mushroom bodies. Science 274, 2104-2107.
645 Cook, R.K., Christensen, S.J., Deal, J.A., Coburn, R.A., Deal, M.E., Gresens, J.M.,
646 Kaufman, T.C., and Cook, K.R. (2012). The generation of chromosomal deletions
647 to provide extensive coverage and subdivision of the Drosophila melanogaster
648 genome. Genome biology 13, R21.
649 Diao, F., Ironfield, H., Luan, H., Diao, F., Shropshire, W.C., Ewer, J., Marr, E., Potter,
650 C.J., Landgraf, M., and White, B.H. (2015). Plug-and-play genetic access to
651 drosophila cell types using exchangeable exon cassettes. Cell reports 10, 1410-
652 1421.
653 Dietzl, G., Chen, D., Schnorrer, F., Su, K.C., Barinova, Y., Fellner, M., Gasser, B.,
654 Kinsey, K., Oppel, S., Scheiblauer, S., *et al.* (2007). A genome-wide transgenic

655 RNAi library for conditional gene inactivation in Drosophila. Nature 448, 151-
656 U151.
657 Hayashi, S., Ito, K., Sado, Y., Taniguchi, M., Akimoto, A., Takeuchi, H., Aigaki, T.,
658 Matsuzaki, F., Nakagoshi, H., Tanimura, T.*, et al.* (2002). GETDB, a database
659 compiling expression patterns and molecular locations of a collection of Gal4
660 enhancer traps. Genesis 34, 58-61.
661 Houseley, J.M., Garcia-Casado, Z., Pascual, M., Paricio, N., O'Dell, K.M., Monckton,
662 D.G., and Artero, R.D. (2006). Noncanonical RNAs from transcripts of the
663 Drosophila muscleblind gene. The Journal of heredity 97, 253-260.
664 Iijima, T., Iijima, Y., Witte, H., and Scheiffele, P. (2014). Neuronal cell type-specific
665 alternative splicing is regulated by the KH domain protein SLM1. The Journal of
666 cell biology 204, 331-342.
667 Irion, U. (2012). Drosophila muscleblind codes for proteins with one and two
668 tandem zinc finger motifs. PloS one 7, e34248.
669 Juni, N., and Yamamoto, D. (2009). Genetic analysis of chaste, a new mutation of
670 Drosophila melanogaster characterized by extremely low female sexual
671 receptivity. Journal of neurogenetics 23, 329-340.
672 Kania, A., Salzberg, A., Bhat, M., D'Evelyn, D., He, Y., Kiss, I., and Bellen, H.J. (1995).
673 P-element mutations affecting embryonic peripheral nervous system
674 development in Drosophila melanogaster. Genetics 139, 1663-1678.
675 Kerwin, S.K., Li, J.S.S., Noakes, P.G., Shin, G.J., and Millard, S.S. (2018). Regulated
676 Alternative Splicing of Drosophila Dscam2 Is Necessary for Attaining the
677 Appropriate Number of Photoreceptor Synapses. Genetics 208, 717-728.
678 Kino, Y., Mori, D., Oma, Y., Takeshita, Y., Sasagawa, N., and Ishiura, S. (2004).
679 Muscleblind protein, MBNL1/EXP, binds specifically to CHHG repeats. Human
680 molecular genetics 13, 495-507.
681 Kuroyanagi, H., Kobayashi, T., Mitani, S., and Hagiwara, M. (2006). Transgenic
682 alternative-splicing reporters reveal tissue-specific expression profiles and
683 regulation mechanisms in vivo. Nature methods 3, 909-915.
684 Lah, G.J., Li, J.S., and Millard, S.S. (2014). Cell-specific alternative splicing of
685 Drosophila Dscam2 is crucial for proper neuronal wiring. Neuron 83, 1376-1388.
686 Lai, S.L., and Lee, T. (2006). Genetic mosaic with dual binary transcriptional
687 systems in Drosophila. Nature neuroscience 9, 703-709.
688 Lee, T., and Luo, L. (1999). Mosaic analysis with a repressible cell marker for
689 studies of gene function in neuronal morphogenesis. Neuron 22, 451-461.
690 Li, J.S., Shin, G.J., and Millard, S.S. (2015). Neuronal cell-type-specific alternative
691 splicing: A mechanism for specifying connections in the brain? Neurogenesis 2,
692 e1122699.
693 Li, L.B., Yu, Z., Teng, X., and Bonini, N.M. (2008). RNA toxicity is a component of
694 ataxin-3 degeneration in Drosophila. Nature 453, 1107-1111.
695 Llamusi, B., Bargiela, A., Fernandez-Costa, J.M., Garcia-Lopez, A., Klima, R.,
696 Feiguin, F., and Artero, R. (2013). Muscleblind, BSF and TBPH are mislocalized in
697 the muscle sarcomere of a Drosophila myotonic dystrophy model. Disease
698 models & mechanisms 6, 184-196.
699 Markovtsov, V., Nikolic, J.M., Goldman, J.A., Turck, C.W., Chou, M.Y., and Black, D.L.
700 (2000). Cooperative assembly of an hnRNP complex induced by a tissue-specific
701 homolog of polypyrimidine tract binding protein. Molecular and cellular biology
702 20, 7463-7479.

703 Millard, S.S., Flanagan, J.J., Pappu, K.S., Wu, W., and Zipursky, S.L. (2007). Dscam2
704 mediates axonal tiling in the Drosophila visual system. Nature 447, 720-724.
705 Millard, S.S., Lu, Z., Zipursky, S.L., and Meinertzhagen, I.A. (2010). Drosophila
706 dscam proteins regulate postsynaptic specificity at multiple-contact synapses.
707 Neuron 67, 761-768.
708 Mondal, K., VijayRaghavan, K., and Varadarajan, R. (2007). Design and utility of
709 temperature-sensitive Gal4 mutants for conditional gene expression in
710 Drosophila. Fly 1, 282-286.
711 Nern, A., Pfeiffer, B.D., and Rubin, G.M. (2015). Optimized tools for multicolor
712 stochastic labeling reveal diverse stereotyped cell arrangements in the fly visual
713 system. Proceedings of the National Academy of Sciences of the United States of
714 America 112, E2967-E2976.
715 Newsome, T.P., Schmidt, S., Dietzl, G., Keleman, K., Asling, B., Debant, A., and
716 Dickson, B.J. (2000). Trio combines with dock to regulate Pak activity during
717 photoreceptor axon pathfinding in Drosophila. Cell 101, 283-294.
718 Ni, J.Q., Markstein, M., Binari, R., Pfeiffer, B., Liu, L.P., Villalta, C., Booker, M.,
719 Perkins, L., and Perrimon, N. (2008). Vector and parameters for targeted
720 transgenic RNA interference in Drosophila melanogaster. Nature methods 5, 49-
721 51.
722 Nilsen, T.W., and Graveley, B.R. (2010). Expansion of the eukaryotic proteome by
723 alternative splicing. Nature 463, 457-463.
724 Norris, A.D., Gao, S., Norris, M.L., Ray, D., Ramani, A.K., Fraser, A.G., Morris, Q.,
725 Hughes, T.R., Zhen, M., and Calarco, J.A. (2014). A pair of RNA-binding proteins
726 controls networks of splicing events contributing to specialization of neural cell
727 types. Molecular cell 54, 946-959.
728 Ohno, G., Hagiwara, M., and Kuroyanagi, H. (2008). STAR family RNA-binding
729 protein ASD-2 regulates developmental switching of mutually exclusive
730 alternative splicing in vivo. Genes & development 22, 360-374.
731 Pan, Q., Shai, O., Lee, L.J., Frey, B.J., and Blencowe, B.J. (2008). Deep surveying of
732 alternative splicing complexity in the human transcriptome by high-throughput
733 sequencing. Nature genetics 40, 1413-1415.
734 Parks, A.L., Cook, K.R., Belvin, M., Dompe, N.A., Fawcett, R., Huppert, K., Tan, L.R.,
735 Winter, C.G., Bogart, K.P., Deal, J.E., *et al.* (2004). Systematic generation of high-
736 resolution deletion coverage of the Drosophila melanogaster genome. Nature
737 genetics 36, 288-292.
738 Pascual, M., Vicente, M., Monferrer, L., and Artero, R. (2006). The Muscleblind
739 family of proteins: an emerging class of regulators of developmentally
740 programmed alternative splicing. Differentiation; research in biological diversity
741 74, 65-80.
742 Schreiner, D., Nguyen, T.M., Russo, G., Heber, S., Patrignani, A., Ahrne, E., and
743 Scheiffele, P. (2014). Targeted combinatorial alternative splicing generates brain
744 region-specific repertoires of neurexins. Neuron 84, 386-398.
745 Spradling, A.C., Stern, D., Beaton, A., Rhem, E.J., Laverty, T., Mozden, N., Misra, S.,
746 and Rubin, G.M. (1999). The Berkeley Drosophila Genome Project gene
747 disruption project: Single P-element insertions mutating 25% of vital Drosophila
748 genes. Genetics 153, 135-177.
749 Tadros, W., Xu, S.W., Akin, O., Yi, C.H., Shin, G.J.E., Millard, S.S., and Zipursky, S.L.
750 (2016). Dscam Proteins Direct Dendritic Targeting through Adhesion. Neuron
751 89, 480-493.

752 Tomioka, M., Naito, Y., Kuroyanagi, H., and Iino, Y. (2016). Splicing factors control
753 C. elegans behavioural learning in a single neuron by producing DAF-2c receptor.
754 Nature communications 7, 11645.
755 Underwood, J.G., Boutz, P.L., Dougherty, J.D., Stoilov, P., and Black, D.L. (2005).
756 Homologues of the Caenorhabditis elegans Fox-1 protein are neuronal splicing
757 regulators in mammals. Molecular and cellular biology 25, 10005-10016.
758 Venken, K.J., Schulze, K.L., Haelterman, N.A., Pan, H., He, Y., Evans-Holm, M.,
759 Carlson, J.W., Levis, R.W., Spradling, A.C., Hoskins, R.A., and Bellen, H.J. (2011).
760 MiMIC: a highly versatile transposon insertion resource for engineering
761 Drosophila melanogaster genes. Nature methods 8, 737-743.
762 Vicente, M., Monferrer, L., Poulos, M.G., Houseley, J., Monckton, D.G., O'Dell K, M.,
763 Swanson, M.S., and Artero, R.D. (2007). Muscleblind isoforms are functionally
764 distinct and regulate alpha-actinin splicing. Differentiation; research in biological
765 diversity 75, 427-440.
766 Wang, E.T., Cody, N.A., Jog, S., Biancolella, M., Wang, T.T., Treacy, D.J., Luo, S.,
767 Schroth, G.P., Housman, D.E., Reddy, S.*, et al.* (2012). Transcriptome-wide
768 regulation of pre-mRNA splicing and mRNA localization by muscleblind proteins.
769 Cell 150, 710-724.
770 Wang, E.T., Sandberg, R., Luo, S., Khrebtukova, I., Zhang, L., Mayr, C., Kingsmore,
771 S.F., Schroth, G.P., and Burge, C.B. (2008). Alternative isoform regulation in
772 human tissue transcriptomes. Nature 456, 470-476.
773 Warzecha, C.C., Sato, T.K., Nabet, B., Hogenesch, J.B., and Carstens, R.P. (2009).
774 ESRP1 and ESRP2 are epithelial cell-type-specific regulators of FGFR2 splicing.
775 Molecular cell 33, 591-601.
776 Xu, T., and Rubin, G.M. (1993). Analysis of genetic mosaics in developing and
777 adult Drosophila tissues. Development 117, 1223-1237.
778

Li et al. Figure 1.

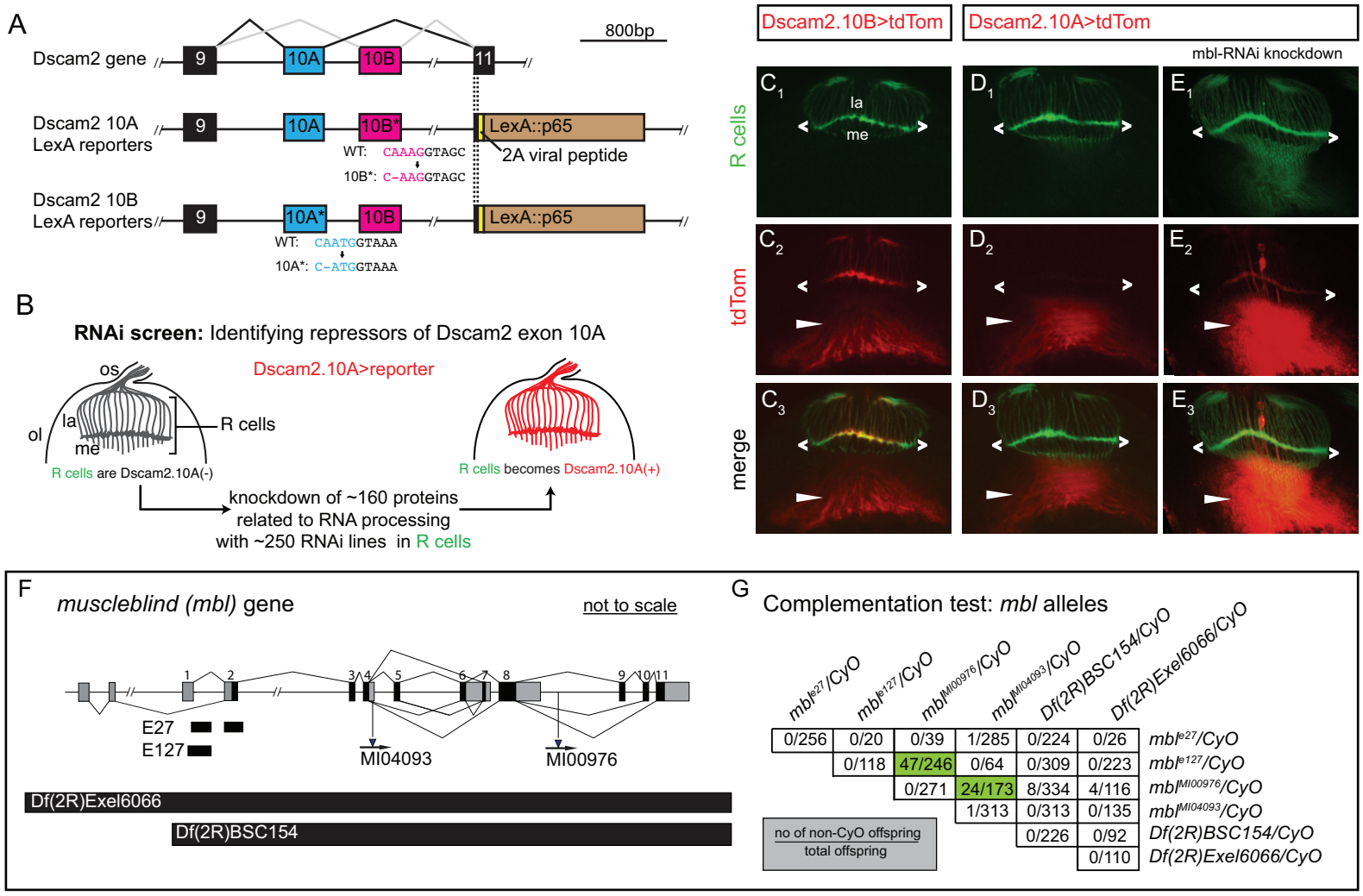

Li et al. Figure 2.

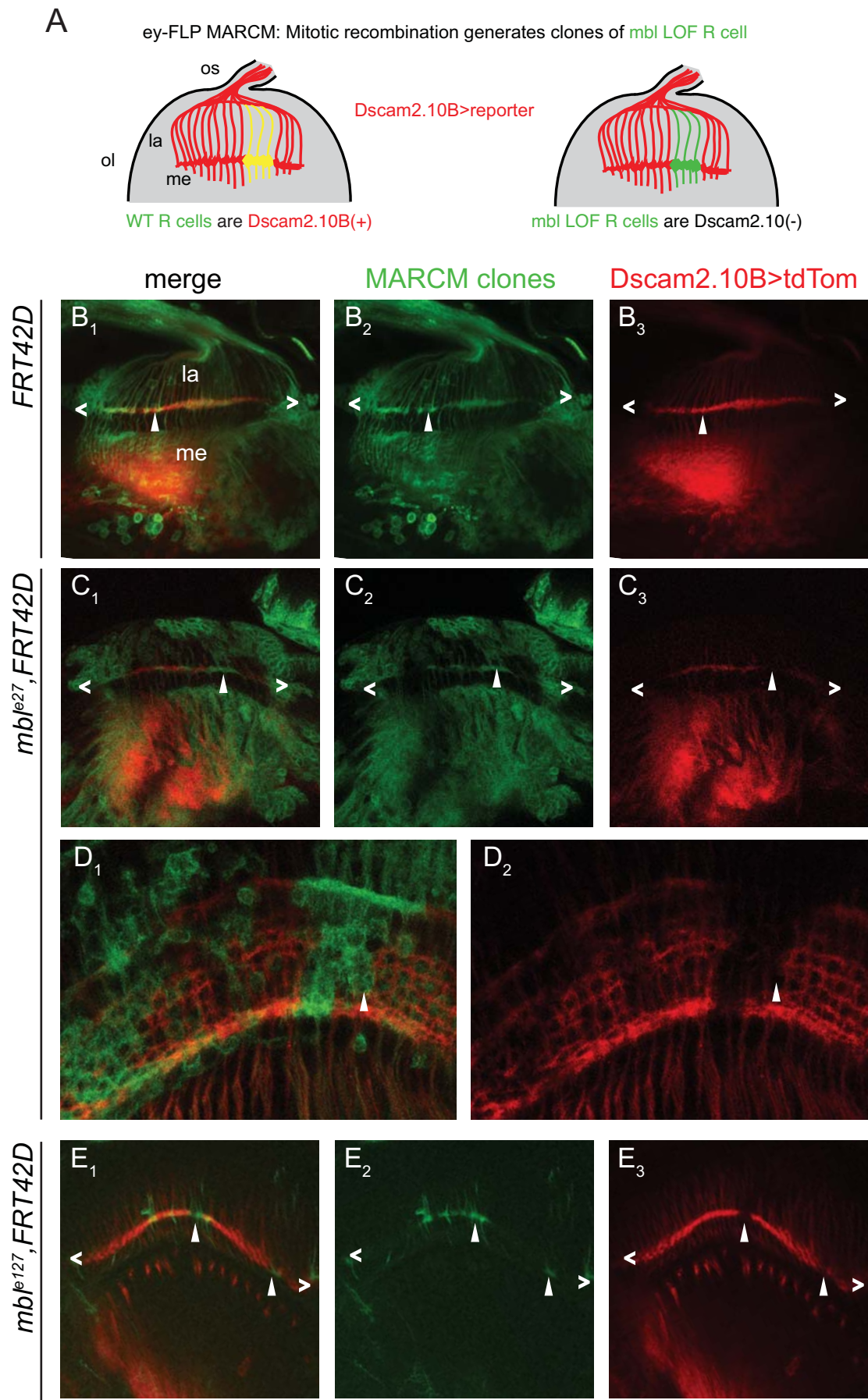

Li et al. Figure 3.

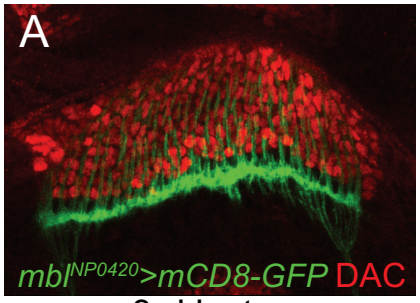

3rd instar

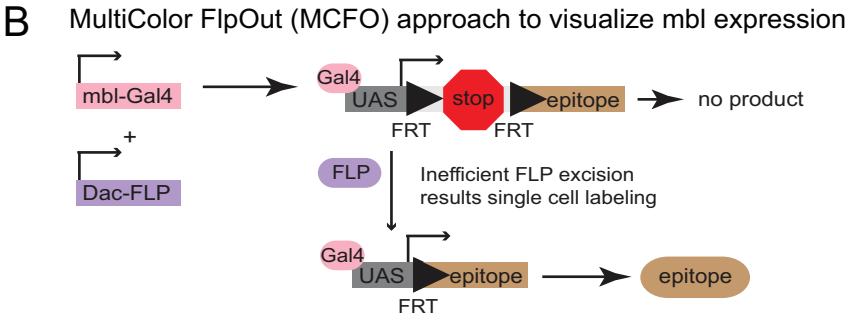

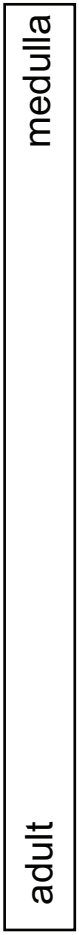

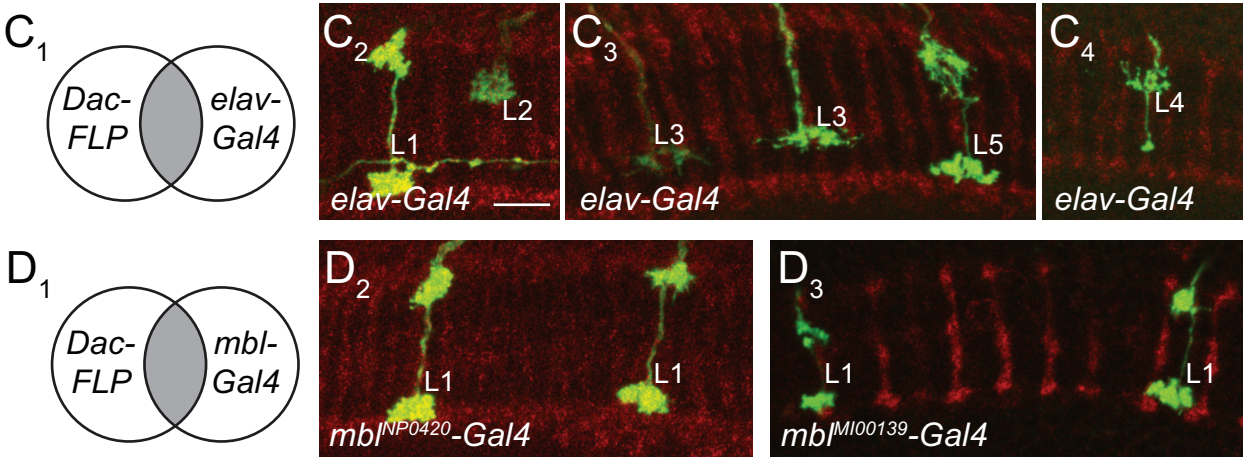

E

	Genotype	L1	L2	L3	L4	L5	R7	R8	Total	no. of OLs
Dac-FLP(III), UAS>stop>epitope	elav-Gal4	71	125	69	39	93	12	28	437	37
	mblNP0420-Gal4	238	0	0	4	0	76	146	464	48
	mblMI00139-Gal4	95	0	0	0	0	111	210	416	61
	Dscam2 10A-Gal4	0	119	115	58	145	0	0	437	32
	Dscam2 10B-Gal4	251	0	0	138	0	16	55	460	21

Many clones detected
Few clones detected
No clones detected

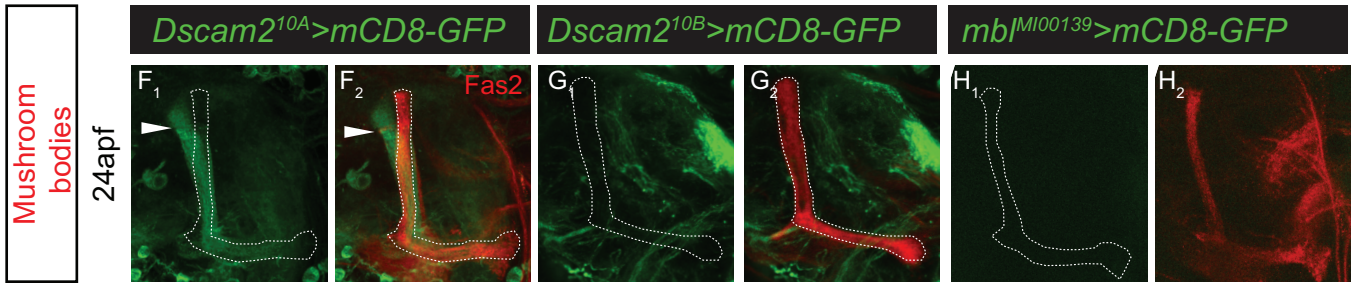

Li et al. Figure 4.

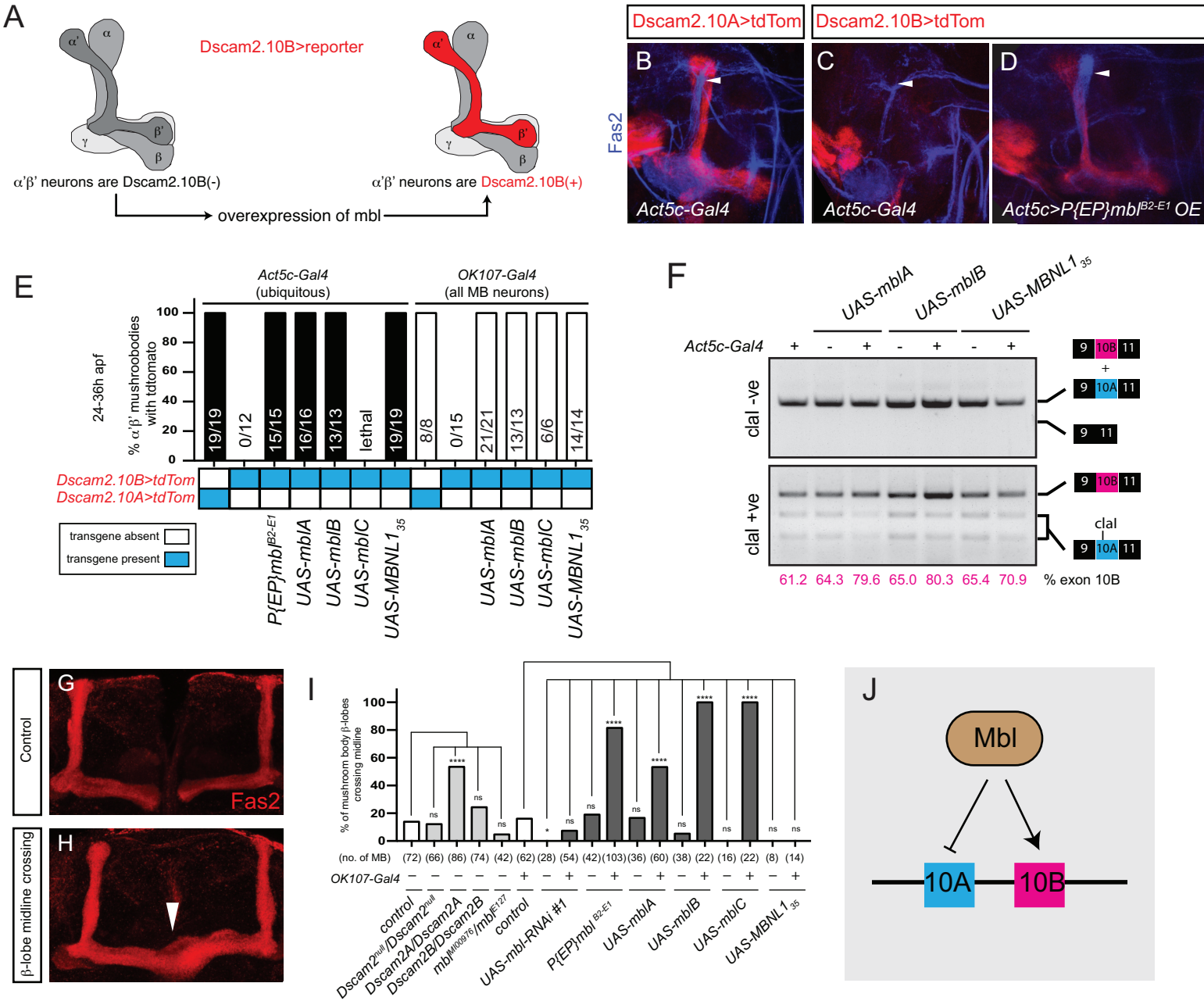

Figure S1. Related to Figure 1. *Mbl* LOF results in aberrant *Dscam2*.10A reporter expression in eye mosaic clones.

(A-F) Eye mosaics of *mbl* LOF alleles cause derepression of *Dscam2.10A>tdTom* in R cells. *WT* mosaic clones (GFP-negative) express *Dscam2.10B>tdTom* (A_1-A_4) but not *Dscam2.10A>tdTom* (B_1-B_4). *Mbl* mutant (GFP-negative) clones, *Df(2R)BSC154* show aberrant *Dscam2.10A* expression in R cells (C_1-C_4). (D) mbl^{e27} eye clones exhibit derepression of Dscam2.10A (red). (E) Clones of a *mbl* allele that deleted only a portion of all mbl isoforms ($mbl^{MI00976}$) do not exhibit derepression of Dscam2.10A. (F) Quantification of *Dscam2.10>tdTom* expression in third instar R cells with *mbl* LOF eye mosaic clones. Y-axis represents the number of optic lobes with R cells positive for tdTom over total number of optic lobes quantified as a percentage. On the x-axis, the presence of a transgene is indicated with a blue box.

Figure S2. Related to Figure 1. *Mbl* LOF does not affect other *Dscam2* splicing events.

(A) *Mbl* LOF does not affect other *Dscam2* splicing events. Semiquantitative RT-PCR from different genotypes indicated. Primers amplified the variable region that includes exon 19S/19L or three alternative last exons (ALE). Percentage of 19L inclusion was calculated by dividing the 19L band by 19L+19S. Percentage of ALE 21A and ALE 21BL inclusion was calculated by dividing respectively the 21A and 21BL band by 21A+21BL+21BS (total). (B) Graphs of RT-PCR data from L. Plots show minimum (bottom line), mean (middle line) and maximum (top line) points, where individual points depict biological replicates. Dashed line represents mean of control.

Figure S3. Related to Figure 3. *Mbl* is expressed in R cells, neurons and glia

(A) Schematic showing the insertion locations of different *mbl* reporters. Translated regions (black) and non-translated regions (grey) are shown.

(B) *Mbl* is expressed in R cells (red) in third instar eye-discs (ed). The *mbl* splicing trap reporter (green*)* overlapped with a marker of R cells (24B10).

(C-G) $mbl^{MI00139}$>*GFP.nls* is expressed in neurons and muscles. (C_1-C_2) Representative confocal image of a $mbl^{MI00139}$>*GFP.nls* (green) adult brain co-labelled with an ELAV antibody (red). Dashed lines demarcate GFP(+) cells. Yellow solid arrowheads show GFP(+) cells that are ELAV(-). (D) Quantification of *mbl* in third instar and adult brains where ~90-100% of GFP(+) cells are also ELAV(+) (black bars). Y-axis represents the number of GFP(+) cells positive for ELAV quantified as a percentage. (E_1-E_2) Representative confocal image of a $mbl^{MI00139}$>*GFP.nls* adult brain labelled with a Repo antibody (red). Dashed lines demarcate GFP(+) cells. White solid arrowheads show GFP(+) cells that are positive for Repo. (F) Quantification of $mbl^{MI00139}$>*GFP.nls* where ~0-10% of $mbl^{MI00139}$>*GFP.nls* (+) cells are also Repo(+).Y-axis represents the number of GFP(+) cells positive for Repo quantified as a percentage. (G_1-G_2) $mbl^{MI00139}$>*GFP.nls* expression is also found in third instar muscles m4-m8, m12 and m13 (Phalloidin, red).

(H_1-H_2) Representative confocal image of a mbl^{NP0420}>*GFP.nls* (green) adult brain co-labelled with an ELAV antibody (red). Dashed lines demarcate GFP(+) cells. (I) Quantification of mbl^{NP0420}>*GFP.nls* in third instar and adult brains where ~80-90% of GFP(+) cells are also ELAV(+). (J-K) In third instar and adult brains, mbl^{NP0420}>*GFP.nls* overlaps minimally with Repo (red). (J_1-J_2) Representative confocal image of a mbl^{NP0420}>*GFP.nls* adult brain labelled with Repo. Dashed lines demarcate GFP(+) cells. White solid arrowheads show GFP(+) cells that are positive

for Repo. (K) Quantification of *mbl*^{NP0420}>*GFP.nls* in third instar and adult brains where ~10-15% of GFP (+) cells are also Repo(+). (L_1-L_2) *mbl*^{NP0420}>*GFP.nls* expression is not detected in third instar muscles m4-m8, m12 and m13 (Phalloidin, red).

Figure S4. Related to Figure 3. *Mbl* expression is cell-type-specific and correlates with *Dscam2.10B*.

(A) Quantification of lamina neurons and R7-R8 neurons observed using the intersectional strategy during development. Two different *mbl* reporters were used. The transcriptional reporter labelled L4 cells early in development whereas the splicing trap reporter did not. This is most likely due to the lower efficiency of the splicing trap given that it produced 5X fewer L1 clones at 72hr compared to the transcriptional reporter. Blue boxes represent detection of reporter expression at different hours after pupal formation (apf). (B) A plot of the percentage of L4 lamina neurons over total lamina neurons during development (data from the *mbl* transcriptional reporter).

(C-E) *Mbl* is not detected in MB neurons that express *Dscam2.10A* in adults. (C_1-C_2) *Dscam2.10A* is expressed in α'β' mushroom body neurons (asterisks) but not the αβ and γ subsets of MB neurons labelled by Fas2 (red). Neither *Dscam2.10B* (D_1-D_2) nor *mbl* (E_1-E_2) are expressed in MB neurons. Neurons in the midline express both *Dscam2.10B* and *mbl* (white arrowhead).

Li et al. Figure S1.

3rd instar
Eye mosaics (ey-FLP)

Dscam2.10B>tdTom | Dscam2.10A>tdTom

FRT42D | Df(2R)BSC154, FRT42D

A1 B1 C1
A2 B2 C2
A3 B3 C3
A4 B4 C4

mbl^e27,FRT42D | mbl^MI00976,FRT42D

D E

F

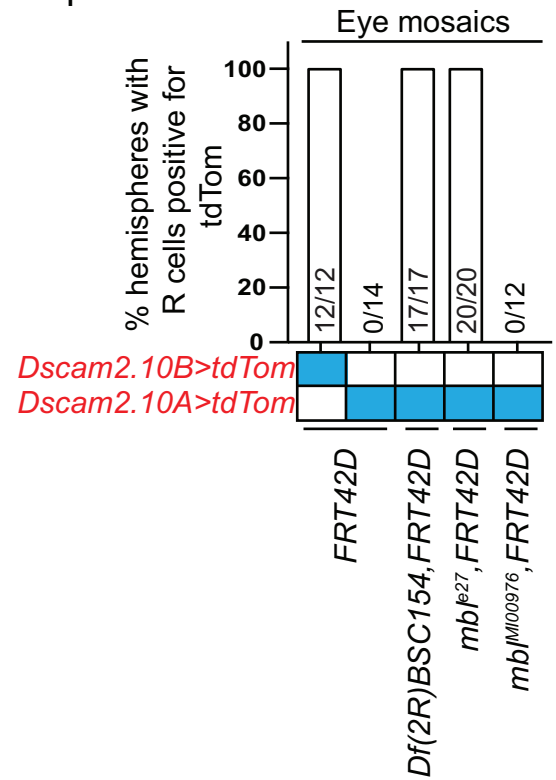

Li et al. Figure S2.

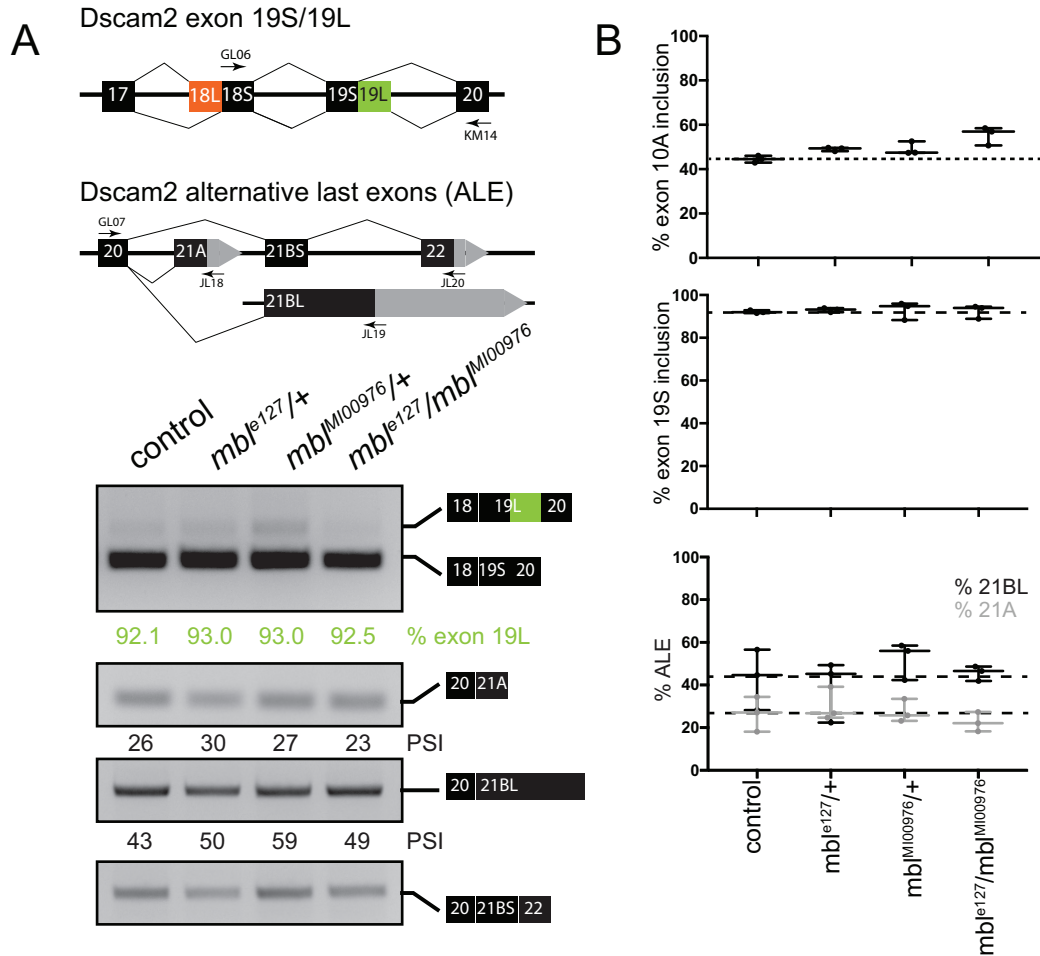

Li et al. Figure S3.

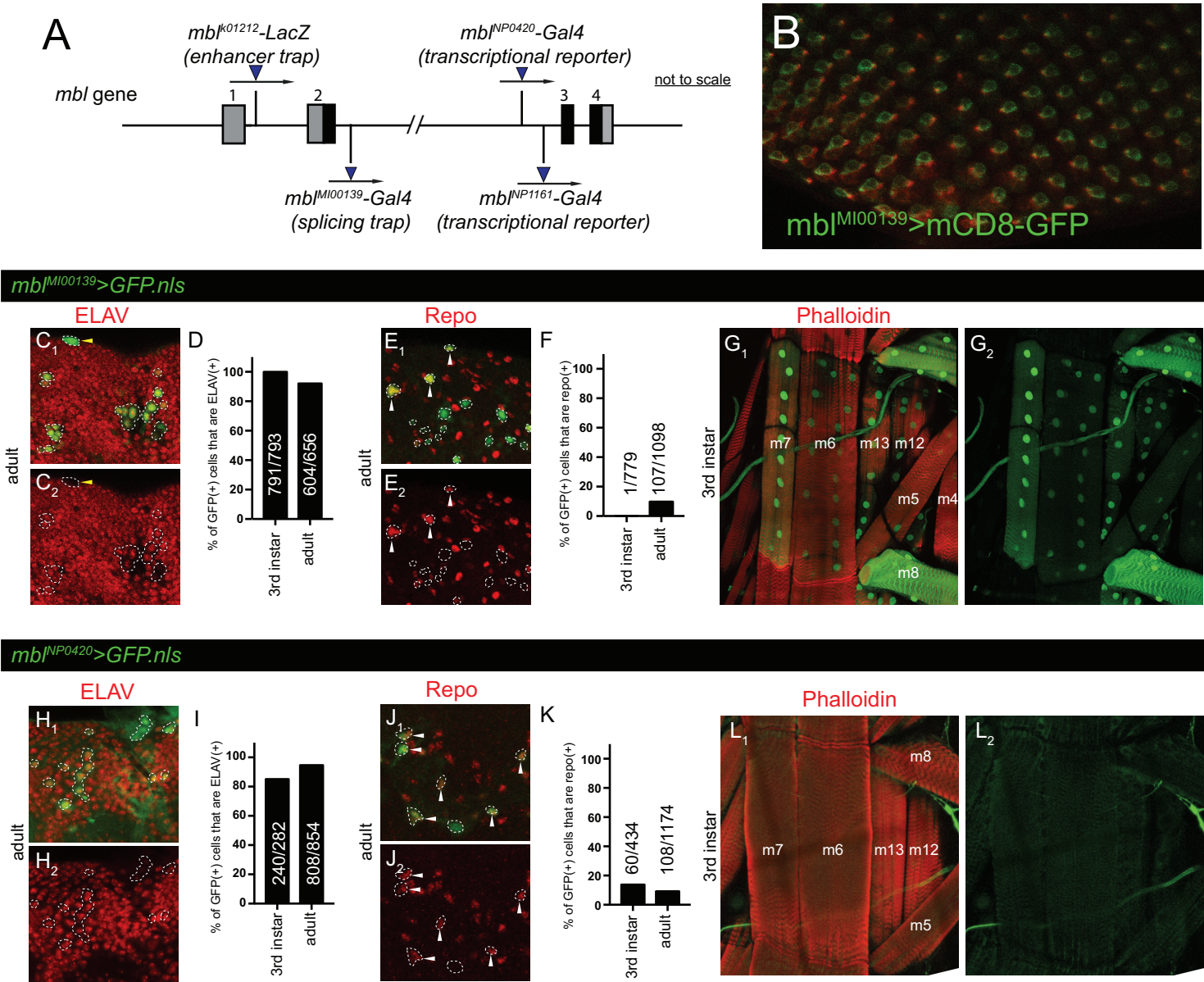

Li et al. Figure S4.

A

	Genotype		L1	L2	L3	L4	L5	R7	R8	Total	no. of OLs
Dac-FLP(III), UAS>stop>epitope	*mbl*^{NP0420}*-Gal4*	72 apf	75	0	0	10	0	10	38	133	8
		60 apf	22	0	0	8	0	15	29	74	8
		48 apf	7	0	0	3	0	1	9	20	2
	mbl^{MI00139}*-Gal4*	72 apf	15	0	0	0	0	6	15	36	8
		48 apf	12	0	0	0	0	4	24	40	8

Clones detected

No clones detected

B

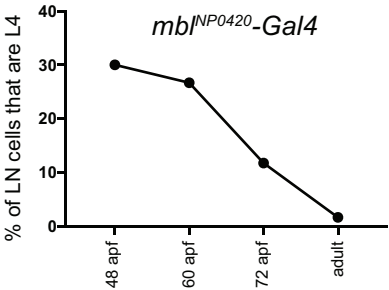

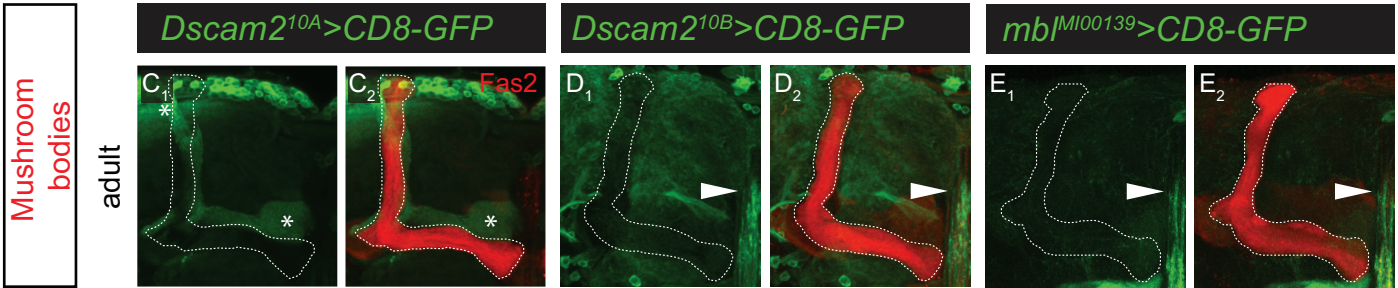

Table S1. List of tested RNAi that did not de-repress Dscam2 exon 10A in R cells

Flybase Number	CG Number	Gene Name	RNAi ID	no. of ol/ed	no. of animals
FBgn0052062	CG32062	A2bp1	27286	12	6
FBgn026239	CG6671	AGO1	33727	3	2
FBgn0000114	CG31762	aret	44483	18	9
FBgn0004587	CG10851	B52	v38862	16	8
FBgn0004587	CG10851	B52	v38860	4	2
FBgn0037660	CG18005	beag	v103832	8	4
FBgn0015907	CG13425	bl	v2912	10	6
FBgn0015907	CG13425	bl	v105271	9	5
FBgn0262475	CG6319	bru-2	50631	13	7
FBgn0264001	CG43744	Bru-3	50734	8	4
FBgn0031883	CG11266	Caper	55742	10	6
FBgn0031883	CG11266	Caper	55742	8	4
FBgn0022942	CG7035	Cbp80	v22331	12	8
FBgn0035136	CG6905	Cdc5	v13492	2	1
FBgn0035136	CG6905	Cdc5	v109369	10	5
FBgn0032690	CG10333	CG10333	v18132	12	8
FBgn0032690	CG10333	CG10333	v18133	4	2
FBgn0036277	CG10418	CG10418	v105940	11	6
FBgn0037531	CG10445	CG10445	v104753	14	7
FBgn0036314	CG10754	CG10754	v31346	11	8
FBgn0039920	CG11360	CG11360	v38491	15	8
FBgn0039920	CG11360	CG11360	v38492	11	6
FBgn0035692	CG13298	CG13298	55257	8	4
FBgn0035162	CG13900	CG13900	v18955	9	6
FBgn0035163	CG13900	CG13900	v108248	16	8
FBgn0037220	CG14641	CG14641	v110507/CyOtb	11	6
FBgn0038464	CG16941	CG16941	v20338	1	1
FBgn0033089	CG17266	CG17266	v25243	10	5
FBgn0033089	CG17266	CG17266	v25244	2	1
FBgn0029751	CG17764	CG17764	v20541	12	7
FBgn0029751	CG17764	CG17764	v101894	10	5
FBgn0035271	CG2021	CG2021	28579	8	5
FBgn0031266	CG2807	CG2807	v25162	8	5
FBgn0037344	CG2926	CG2926	v33589	11	5
FBgn050122	CG30122	CG30122	55209	6	3
FBgn0031631	CG3225	CG3225	v24725	9	5
FBgn0052533	CG32533	CG32533	v38634	1	1
FBgn0052533	CG32533	CG32533	v51785	11	6
FBgn0031628	CG3294	CG3294	v26111/TM6B	12	6
FBgn0031628	CG3294	CG3294	v26111/TM6B	12	6
FBgn0053108	CG33108	CG33108	v24996	9	5
FBgn0031229	CG3436	CG3436	55207/CyOtb	4	2
FBgn0031492	CG3542	CG3542	v26227	10	5
FBgn0031492	CG3542	CG3542	v26229	4	2
FBgn0031493	CG3605	CG3605	v26250	12	7
FBgn0031493	CG3605	CG3605	v26252	8	5
FBgn0035987	CG3689	CG3689	v45278	10	5
FBgn0028474	CG4119	CG4119	v26395	9	5
FBgn0028474	CG4119	CG4119	v106696/CyOtb	10	6
FBgn0034598	CG4266	CG4266	v26472	14	7
FBgn0034598	CG4266	CG4266	v26475	4	2
FBgn0031287	CG4291	CG4291	v21819/TM6B	11	6
FBgn0035016	CG4612	CG4612	v52497	9	5
FBgn0039566	CG4849	CG4849	v21962	9	5
FBgn0032194	CG4901	CG4901	v34904	11	6
FBgn0038344	CG5205	CG5205	v107282	9	5
FBgn0039182	CG5728	CG5728	v24697	14	7
FBgn0038927	CG6015	CG6015	34565	lethal	
FBgn0030631	CG6227	CG6227	v40351	11	8
FBgn0030632	CG6227	CG6227	v40352	12	6
FBgn0004903	CG6354	CG6354	31333	12	9
FBgn0004903	CG6354	CG6354	55662	8	4
FBgn0035675	CG6610	CG6610	v106830	10	6
FBgn0035675	CG6610	CG6610	31870	10	6
FBgn0036828	CG6841	CG6841	v34253/CyOtb	10	5
FBgn0030085	CG6999	CG6999	v110143	11	7
FBgn0030085	CG6999	CG6999	55157	12	6
FBgn0035872	CG7185	CG7185	v107147	5	3
FBgn0035872	CG7185	CG7185	34804	14	7
FBgn0036734	CG7564	CG7564	v100562	10	5
FBgn0035235	CG7879	CG7879	56930	10	5
FBgn0038887	CG7907	CG7907	55370	6	3
FBgn0035253	CG7971	CG7971	v101384	10	7
FBgn0027567	CG8108	CG8108	v35344	12	7
FBgn0030697	CG8565	CG8565	v100449	10	7
FBgn0030697	CG8565	CG8565	55368	11	6
FBgn0032883	CG9323	CG9323	v44984	12	8
FBgn0032883	CG9323	CG9323	v110410	8	4
FBgn0015621	CG3642	Clp	v26259	12	7
FBgn0015621	CG3642	Clp	v26261	13	7
FBgn0263995	CG43738	cpo	28360	8	4
FBgn0027873	CG1957	Cpsf100	50893/TM6B	8	5
FBgn0027873	CG1957	Cpsf100	50893/TM6B	8	5
FBgn0024698	CG10110	Cpsf160	v18009	11	6
FBgn0024698	CG10110	Cpsf160	v110571	9	6
FBgn0261065	CG7698	Cpsf73	v39558	9	5
FBgn0000377	CG3193	crn	v25919	lethal	
FBgn0039867	CG2261	CstF-50	v43716	10	5
FBgn0039867	CG2261	CstF-50	v109583	8	4
FBgn0027841	CG7697	CstF-64	v21045/CyOtb	10	6
FBgn0010220	CG12759	Dbp45A	v17306	6	3
FBgn0010221	CG12760	Dbp45A	v104183	13	7
FBgn0033160	CG11107	Dhx15	v44119/CyOtb	10	6
FBgn0031601	CG3058	Dim1	v21258	10	5
FBgn0259220	CG42320	Doa	v19066	9	5
FBgn0020306	CG9696	dom	v7787	2	1
FBgn0000562	CG4051	egl	28969	8	4
FBgn0001942	CG9075	eIF-4a	v42202	lethal	
FBgn0034237	CG4878	eIF3-S9	32880	lethal	
FBgn0260400	CG4262	elav	28371	2	1
FBgn0033859	CG6197	fand	v104186	10	5
FBgn0036850	CG10419	Gem2	v47372	13	8
FBgn0036850	CG10419	Gem2	v47374	10	7
FBgn0259139	CG6946	glo	33668	9	6
FBgn0259139	CG6946	glo	v27752	12	6
FBgn0001179	CG8019	hay	v41023	12	8
FBgn0014189	CG7269	Hel25E	v22557	9	5
FBgn0011224	CG31000	heph	v33735	10	6
FBgn0011224	CG31000	heph	v110749	18	10
FBgn0264491	CG10293	how	v13756	13	7
FBgn0264491	CG10293	how	v100775	10	5
FBgn0004838	CG10377	Hrb27c, Hrp48	v16040	12	7
FBgn0004838	CG10377	Hrb27c, Hrp48	31685	6	3
FBgn0004838	CG10377	Hrb27c, Hrp48	33716	8	4
FBgn0004237	CG12749	Hrb87F, hrp36	v51759	9	6
FBgn0004237	CG12749	Hrb87F, hrp36	52937	11	6
FBgn0004237	CG12749	Hrb87F, hrp36	31244	14	8
FBgn0001215	CG9983	Hrb98DE, hrp38	31303	10	7
FBgn0001215	CG9983	Hrb98DE, hrp38	32351	13	8
FBgn0015949	CG9854	hrg	v42283	12	6
FBgn0002431	CG9484	hyd	v44675	12	6
FBgn0039691	CG1972	IntS11	v33450	7	5
FBgn0039691	CG1972	IntS11	v109408	8	5
FBgn0036570	CG5222	IntS9	v110367	10	5
FBgn0026713	CG32604	l(1)G0007	v31908	15	8
FBgn0026714	CG32605	l(1)G0008	v31909	4	2
FBgn0086444	CG10689	l(2)37Cb	v31324	9	6
FBgn0263599	CG5931	l(3)72Ab	v43962	5	3
FBgn0263600	CG5932	l(3)72Ab	v110666	6	3
FBgn0035838	CG7942	ldbr	v110582	8	5
FBgn0035838	CG7942	ldbr	55661	8	6
FBgn0034834	CG3162	LS2	v21379	11	7
FBgn0034834	CG3162	LS2	v21380	14	7
FBgn0261067	CG4279	LSm1	v28793	11	6
FBgn0261067	CG4279	LSm1	v50653	10	5
FBgn0033450	CG12924	Lsm11	v108336	12	6
FBgn0051184	CG31184	LSm3	56892	4	2
FBgn0261068	CG13277	Lsm7	v23862	10	6
FBgn0011666	CG5099	msi	55152	10	5
FBgn0262737	CG7437	mub	v28024	16	9
FBgn0014366	CG2925	noi	v20943	9	5
FBgn0015520	CG10328	nonA-I	v101567	7	4
FBgn0015520	CG10328	nonA-I	52934	3	2
FBgn0261619	CG5119	pAbp	v22007	9	5
FBgn0005648	CG2163	Pabp2	v106466	10	5
FBgn0086895	CG8241	pea	v47782	9	5
FBgn0027784	CG6011	Prp18	v13760	10	6
FBgn0027784	CG6011	Prp18	v100287	2	1
FBgn0261119	CG5519	Prp19	v108575	11	6
FBgn0261119	CG5519	Prp19	v41438	3	2
FBgn0036915	CG7757	Prp3	v25548	9	6
FBgn0036487	CG6876	Prp31	v35131	3	2
FBgn0036487	CG6876	Prp31	v103721	6	3
FBgn0033688	CG8877	Prp8	v18565	12	7
FBgn0261552	CG42670	Ps	v44710	18	9
FBgn0261552	CG42670	Ps	v24214	10	5
FBgn0014870	CG8912	Psi	v28989	16	8
FBgn0014870	CG8912	Psi	v28990	10	5
FBgn0014870	CG8912	Psi	v105135	10	7
FBgn0028577	CG12085	pUf68	v109796	8	4
FBgn0003165	CG9755	pum	36676	12	7
FBgn0022987	CG4816	qkr54B	34896	10	5
FBgn0022986	CG3613	qkr58E-1	55159	10	5
FBgn0022985	CG5821	qkr58E-2	55279/CyOtb	6	3
FBgn0022984	CG3584	qkr58E-3	55922	10	5
FBgn0260944	CG17136	Rbp1	v21083/TM6B	12	6
FBgn0260944	CG17136	Rbp1	v110008	11	6
FBgn0030479	CG1987	Rbp1-like	v105883	10	6
FBgn0030479	CG1987	Rbp1-like	44100	4	2
FBgn0260943	CG32169	rbp6	61324/CyOtb	8	4
FBgn0015778	CG9412	rin	33392/TM6B	12	7
FBgn0003261	CG10279	Rm62	v46908/TM6B	12	6
FBgn0037707	CG16788	RnpS1	56910	10	5
FBgn0037707	CG16788	RnpS1	36580	6	3
FBgn0005649	CG5422	Rox8	v100563	10	5
FBgn0005649	CG5422	Rox8	v41439	12	6
FBgn0011305	CG5655	Rsf1	v22186/TM3	15	10
FBgn0267790	CG9373	rump	42665/CyOtb	6	3
FBgn0039229	CG6995	Saf-B	51759		5
FBgn0265298	CG5442	SC35	v40590	5	3
FBgn0265298	CG5442	SC35	v104978	6	3
FBgn0025571	CG5836	SF1	v13426	3	2
FBgn0040284	CG6987	SF2	v27775/TM3	13	7
FBgn0040284	CG6987	SF2	v27776/TM6B	6	4
FBgn0052423	CG32423	shep	43545	4	3
FBgn0002354	CG1420	Slu7	v103587	5	3
FBgn0262601	CG5352	SmB	v40587	3	2
FBgn0262601	CG5352	SmB	v110713	12	6
FBgn0261933	CG10753	SmD1	v31343/TM6B	8	4
FBgn0261933	CG10753	SmD1	v31342	7	4
FBgn0261789	CG1249	SmD2	v31947	4	2
FBgn0261789	CG1249	SmD2	v31946	8	4
FBgn0261789	CG1249	SmD2	v100690	4	2
FBgn0023167	CG8427	SmD3	v35933	8	5
FBgn0261790	CG18591	SmE	v23569	4	2
FBgn0261790	CG18591	SmE	v23570/TM6B	10	5
FBgn0000426	CG16792	SmF	v107644/CyOtb	lethal	
FBgn0000426	CG16792	SmF	26734	12	6
FBgn0036641	CG16725	Smn	v100392	7	4
FBgn0003449	CG4528	snf	51459	16	8
FBgn0003449	CG4528	snf	55914	9	5
FBgn0016978	CG8749	snRNP-U1-70K	v23150	11	8
FBgn0016978	CG8749	snRNP-U1-70K	v23151	10	6
FBgn0261792	CG5454	snRNP-U1-C	v22132	11	6
FBgn0261792	CG5454	snRNP-U1-C	v22133	10	5
FBgn0261791	CG9742	SNRPG	v39256	10	5
FBgn0015818	CG3780	Spx	v40471	9	5
FBgn0015818	CG3780	Spx	v40472	9	5
FBgn0263396	CG16901	sqd, hrp40	v32395	12	6
FBgn0263396	CG16901	sqd, hrp40	31302	20	10
FBgn0036340	CG11274	SRm160	v6439	9	5
FBgn0036340	CG11274	SRm160	v100751	8	4
FBgn0015298	CG4457	Srp19	51160	lethal	
FBgn0024285	CG4602	Srp54	v51088	8	6
FBgn0024285	CG4602	Srp54	55254	9	5
FBgn0026370	CG8174	SRPK	v103416	9	6
FBgn0025702	CG11489	srpk79D	v47544	8	5
FBgn0025702	CG11489	srpk79D	v47545	10	5
FBgn0003520	CG5753	stau	31247	9	5
FBgn0003559	CG17170	su(f)	v110125	6	3
FBgn0003638	CG3019	su(wa)	v25597	12	9
FBgn0003638	CG3019	su(wa)	v104716	10	5
FBgn0264270	CG43770	Sxl	34393	10	5
FBgn0037371	CG2097	Sym	v33470	9	5
FBgn0038826	CG17838	syp	56972	10	5
FBgn0038826	CG17838	syp	v33012	15	9
FBgn0025790	CG10327	TBPH	v38377	7	4
FBgn0025790	CG10327	TBPH	v38379	10	5
FBgn0003741	CG16724	tra	v2560	12	6
FBgn0003742	CG10128	tra2	v8868	9	5
FBgn0039117	CG10210	tst	v38356	8	4
FBgn0039117	CG10210	tst	v108216	12	6
FBgn0033378	CG8781	tsu	55367	11	6
FBgn0033378	CG8781	tsu	28955	9	5
FBgn0033210	CG1406	U2A	v17358/TM6B	9	5
FBgn0033210	CG1406	U2A	v109815	11	6
FBgn0017457	CG3582	U2af38	v110075	9	5
FBgn0017457	CG3582	U2af38	29304	13	7
FBgn0005411	CG9998	U2af50	v24176	11	6
FBgn0005411	CG9998	U2af50	v24177	10	6
FBgn0036733	CG6322	U4-U6-60K	v34242	8	6
FBgn0036733	CG6322	U4-U6-60K	v110393	10	6
FBgn0030354	CG1559	Upf1	43144	12	7
FBgn0028554	CG10203	xl6	v31203	14	8
FBgn0028555	CG10204	xl6	v100226	11	7
FBgn0021895	CG18426	ytr	55704	4	2